

INVESTIGATION OF KeV BETA PARTICLE TRANSPORTATION IN MATTER

by

BRIGHT CHUKWUDI IZUDIKE

Presented to the Faculty of the Graduate School of
The University of Texas at Arlington in Partial Fulfillment
of the Requirements
for the Degree of

MASTER OF SCIENCE IN PHYSICS

THE UNIVERSITY OF TEXAS AT ARLINGTON

August 2015

Copyright © by Bright C. Izudike 2015

All Rights Reserved



Acknowledgements

First of all, I would like to thank Dr. Jin Mingwu, for his constant support and advise. Without him, I would have never been able to complete my work. In the same vein, I would appreciate members of my thesis committee Dr. Jaehoon Yu and Dr. Wei Chen for their support and contributions to this work. Many thanks to the African School of Fundamental Physics and Applications (2012) – Kumasi Ghana- which gave me the opportunity to meet with scientist from all over the world, especially Dr. Jaehoon Yu. Who after several consideration gave me the chance to come over to the UTA to study. I deeply thank also, Timothy Hoffman, for the brilliant input he provided. I thank all the people who gave a hand and my family who lovingly hindered me from getting anything done. They give meaning to my life.

July 22, 2015

Abstract

INVESTIGATION OF KeV BETA PARTICLE TRANSPORTATION IN MATTER

Bright Chukwudi Izudike, MS

The University of Texas at Arlington, 2015

Supervising professor: Jin Mingwu

Nuclear imaging is widely used in medicine for more accurate diagnoses and more effective treatment for cancer. Current emission tomography techniques used in clinics may not efficiently detect cancer at a very early stage partly because of the weak signals from small tumors. Portable nuclear imaging devices can more effectively reveal these small tumors in a close proximity for complete malignant tissue destruction. With the advance of detector technology in high energy physics, the detection of beta particles (positron and electron) from clinical/pre-clinical radiotracers, such as those labeled with Cu-64, may open a new avenue for image-guided treatment of cancer.

In this research we use a high energy particle transportation Monte Carlo simulation toolkit (Geometry And Tracking – 4: Geant4) to simulate Beta particles propagating through matter. To demonstrate how beta particles with the energy of interest transport in human soft tissues and interact with materials used in a gas electron multiplier detector, we simulate electrons and positrons with the energy spectrum of ^{64}Cu (half-life of 12.7 hours; 17.8% β^+ decay with the maximum energy of 0.653 MeV;

and 38.4% β^- decay with the maximum energy of 0.579 MeV) traveling through water (mimicking human soft tissues) and four other materials (air, iron, kapton, and beryllium).

We summarized the profiles of beta particles tracks, ionization patterns, and path lengths a electron beam at 579 KeV and a positrons beam at 653 KeV propagating through aforementioned materials. Tracks of these particles were collected in a step size of 0.05 mm in our simulation with the beam source located at the center of a 1cm x 1cm x 1cm cube full of one type of material. The ranges of beta particles in these materials were also summarized. The beta particles emitted from Cu-64 have a long range in air and are only able to penetrate 1-2 mm of water. Kapton is a better material for detector window than iron or beryllium in terms of less attenuation of the beta particles. This study provided the preliminary data to guide the next step of development of a portable nuclear imaging device and imaging experiments.

Table of Contents

Acknowledgements.....	iii
Abstract	iv
List of Figures.....	viii
List of Tables.....	xii
Chapter 1 Introduction	1
1.1 Radiotracer	4
1.2 Beta Decay	6
1.3 Interaction of Beta Particles with Matter	7
1.4 Geant4-Monte Carlo Simulation	7
Chapter 2 Beta Decay	9
2.1 Interaction of Beta particles in Matter	10
2.1.1 Stopping Power	16
2.2 Transportation of Beta Particles	17
2.3 Detection of Beta Particles	17
2.3.1 GEM Detectors	18
2.3.2 Scintillators	19
2.3.2.1 Inorganic Scintillators	19
2.3.2.2 Organic Scintillators	19
2.3.3 Solid State Detectors	20
Chapter 3 Monte Carlo Simulations	22
3.1 Method and Simulation Procedures	23

3.1.1 Installation of Geant4 Simulation toolkit	23
3.1.2 Considerations for Simulation	23
3.1.3 Simulation Setup and Method	25
3.2 Results	26
3.2.1 Beta Particles in Air	26
3.2.2 Beta Particles in Water	32
3.2.3 Beta Particles in Beryllium	42
3.2.4 Beta Particles in Iron	51
3.2.5 Beta Particles in Kapton	69
Chapter 4 Conclusion	68
4.1 Future Work	70
References	71
Biography	75

List of Figures

Fig 2-1	Beta particle spectra from decaying ^{64}Cu	10
Fig 2-2	A radiative collision between a charged particle and an atom for $b \ll a$	12
Fig 2-3	A hard collision between a charged particle and an atom for $b \approx a$	12
Fig 2-4	A soft collision between a charged particle and an atom for $b \gg a$	13
Fig 3-1	Simulation environment	25
Fig 3-2	Showing over 22000 events registered as electrons (charge -1).....	27
Fig 3-3	The displacement of electrons from the origin along the X(mm) axis.....	27
Fig 3-4	The displacement of electrons from the origin along the Y(mm) axis.....	28
Fig 3-5	The displacement of electrons from the origin along the Z(mm) axis.....	28
Fig 3-6	Energy vs radial distance traveled by electron in air.....	29
Fig 3-7	Number of events registered as positrons in the simulation environment	29
Fig 3-8	The distribution of positrons along the X (mm) axis.....	30
Fig 3-9	The distribution of positrons along the Y (mm) axis.....	31
Fig 3-10	The distribution of positrons along the Z (mm) axis.....	31
Fig 3-11	kinetic energy of Positron vs radial distance traveled in air.....	32
Fig 3-12	Number of events with charge -1 (electrons) in water.....	32
Fig 3-13	A blow up of Fig 3.12 around the origin.....	34
Fig 3-14	Distribution of electrons about the origin along the X axis in water.....	34
Fig 3-15	Distribution of electrons about the origin along the Y axis in water.....	35
Fig 3-16	Distribution of electrons about the origin along the Z axis in water.....	35
Fig 3-17	Energy deposited in water by electrons.....	36
Fig 3-18	Kinetic energy of electrons in water at various depth	36

Fig 3-19	Tracks of 579 KeV electrons projected on the XY plane.....	37
Fig 3-20	A mixed field of electrons, positrons and γ photons.....	37
Fig 3-21	Closer look at Fig. 3.20.....	38
Fig 3-22	Distribution of Positrons along the X axis with a range of about 2.2mm.....	38
Fig 3-23	Distribution of Positrons along the Y axis with a range of about 1.8 mm.....	39
Fig 3-24	Distribution of Positrons along the Z axis with a range of about 2.2mm.....	39
Fig 3-25	Number of events and corresponding Energy deposited in water.....	40
Fig 3-26	Tracks of 653 KeV positrons projected on the XY plane.....	40
Fig 3-27	Kinetic energy of Positrons at various depth in water.....	41
Fig 3-28	Number of events with charge (-1) in beryllium.....	41
Fig 3-29	Number of events with charge (0) in beryllium.....	43
Fig 3-30	Distribution of electrons along the X axis in beryllium.....	43
Fig 3-31	Distribution of electrons along the Y axis in beryllium.....	44
Fig 3-32	Distribution of electrons along the Z axis in beryllium.....	44
Fig 3-33	Energy Deposited by electrons in beryllium.....	45
Fig 3-34	Tracks of electrons in beryllium projected on the XY plane.....	45
Fig 3-35	Kinetic energy of Electrons at various depth in beryllium.....	46
Fig 3-36	3170 positron events in beryllium.....	46
Fig 3-37	Fig. 3.36 zoomed in between -1 and 0.....	47
Fig 3-38	Distribution of Positrons along the X axis with a range of 1.6mm.....	47
Fig 3-39	Distribution of Positrons along the Y axis with a range of 1.4mm.....	48
Fig 3-40	Distribution of Positrons along the Z axis with a range of 1.8mm.....	48
Fig 3-41	Energy deposited in beryllium for both electrons and positron events.....	49

Fig 3-42	Kinetic energy of Positrons at various depth in in beryllium.....	49
Fig 3-43	Tracks of 653 KeV positrons in beryllium projected on the XY plane.....	50
Fig 3-44	Number of events with charge (-1) in iron.....	50
Fig 3-45	Number of events with charge (0) in iron from bremsstrahlung radiation.....	52
Fig 3-46	Distribution of electrons along the X axis in iron.....	52
Fig 3-47	Distribution of electrons along the Y axis in iron.....	53
Fig 3-48	Distribution of electrons along the Z axis in iron.....	53
Fig 3-49	Energy Deposited by electrons in iron.....	54
Fig 3-50	Kinetic energy of Electrons at various depth in iron.....	54
Fig 3-51	Tracks of electrons in iron projected on the XY plane.....	55
Fig 3-52	A mixed field of electrons, positrons and γ photons generated.....	55
Fig 3-53	Distribution of Positrons along the X axis with a range of about 0.2 mm.....	56
Fig 3-54	Distribution of Positrons along the Y axis with a range of about 0.2 mm.....	56
Fig 3-55	Distribution of Positrons along the Z axis with a range of about 0.4 mm.....	57
Fig 3-56	Number of events and corresponding Energy deposited in iron.....	57
Fig 3-57	Kinetic energy of positrons in iron at various depth in iron.....	58
Fig 3-58	Number of events with charge (-1) in Kapton.....	58
Fig 3-59	Number of events with charge (0) in kapton from bremsstrahlung radiation.	60
Fig 3-60	Distribution of electrons along the X axis in kapton.....	60
Fig 3-61	Distribution of electrons along the Y axis in kapton.....	61
Fig 3-62	Distribution of electrons along the Z axis in beryllium.....	61
Fig 3-63	Energy Deposited by electrons in kapton.....	62
Fig 3-64	Kinetic energy of electrons at various depth in kapton.....	62

Fig 3-65	Tracks of electrons projected on the XY plane.....	63
Fig 3-66	A mixed field of electrons, positrons and γ photons.....	63
Fig 3-67	A blow up of Fig 3.66 between -1 and 0.....	64
Fig 3-68	Distribution of Positrons along the X axis.....	64
Fig 3-69	Distribution of Positrons along the Y axis.....	65
Fig 3-70	Distribution of Positrons along the Z axis.....	65
Fig 3-71	Energy Deposited by positrons in kapton	66
Fig 3-72	Kinetic energy of positrons at various depth in kapton.....	66
Fig 3-73	Tracks of 653 KeV positrons in kapton projected on the XY plane.....	67

List of Tables

Table 3-1 Elements and their composition/properties considered for this simulations..	24
Table 3-2 Decay properties for Cu and F considered for simulation.....	28
Table 4-1 Summary of results.....	69

Chapter 1

Introduction

Nuclear medicine is a branch of medical physics that involves the administration of specific radiopharmaceuticals (or “radiotracer”) to patients for diagnostic and therapeutic purposes. The radiotracer can follow physiological, metabolic, and molecular pathways to accumulate and retain in the target tissues during the course of diagnostic imaging or treatment. As a therapeutic tool, radiopharmaceuticals emitting short-range ionizing radiation are used for targeted treatment while minimizing the damage to healthy tissues. While in diagnosis, gamma and positron (generating a pair of 511 KeV gamma photons by annihilating with an electron) emitters with strong penetration capability are usually used for external detectors to interrogate the three-dimensional radiotracer distribution inside the patient. Yet, portable imaging devices are also developed to detect or image short-range radiation, such as beta particles, for image-guided interventions. Nuclear imaging is a functional imaging modality with very high sensitivity to molecular events in the body, which could identify abnormalities at a much earlier stage of a disease than structural imaging, such as X-ray computed tomography (CT).

In nuclear imaging, a typical examination or procedure would involve the introduction of a trace amount of radiopharmaceuticals into the body by injection, swallowing, or inhalation, which can be sufficiently detected by the external detector while keeping radiation exposure to the patient under the safety limit. A radiopharmaceutical is composed of a biologically active compound that acts as a vehicle targeting a specific molecular event in the body and a radioisotope serving as a reporter

to be detected externally. Once the radiotracer reaches high uptake in the target site and clears out of the uninterested regions, special detectors are then used to detect radiation emitted by the radioisotope in the radiopharmaceutical, with spatial location (and temporal) information. Images can then be produced by using different modalities, such as Scintigraphy, Positron Emission Tomography (PET) and Single Positron Emission Tomography (SPECT).

PET, is a functional medical imaging technique that can be used to image biochemical or physiological processes within the body. Such images can be acquired by imaging the decay of radio isotopes bound to molecules with known biological properties [1]. PET scanners, for example, rely on radioisotopes, which decay via beta plus decay releasing a positron. The positron annihilates with a nearby electron to produce two 511 KeV γ rays (almost) back to back. A detector ring surrounding the patient could detect the photon pair arriving coincidentally at opposite sides of the detectors. The advent of tomographic reconstruction methods and the development of detector technologies, has made it possible to generate images from the detection of the two 511 KeV photons. Such images provide us with enough information and thus make it possible to follow the dynamics of the tracers in the body with high sensitivity [2,3]. PET is usually performed for cancer diagnosis, staging, and prognosis using glucose analogue, fluorine-18 labeled fluorodeoxyglucose (^{18}F -FDG). Because cancerous cells are more metabolically active and divide more rapidly than normal cells, radiopharmaceuticals targeting glucose metabolism are effective to detect cancerous tumors. Since changes in metabolic activities could characterize cancer progression better than anatomical imaging, ^{18}F -FDG

PET is widely used for cancer imaging.

SPECT uses one to three gamma cameras which rotate around the patient to detect gamma photons emitted from a gamma emitter. The radioisotopes used in SPECT usually are easier to make and have longer half lives than those used in PET scans. Each decay emits one γ photon, whose direction can be determined by using a collimator.

PET and SPECT are limited by a lack of anatomical details. The integration of PET and SPECT with CT or magnetic resonance imaging (MRI) . However, the low resolution and bulky size of these scanners are not suitable to detect small tumors (in mm size) in an operation room.

Gamma (γ) and beta (β) portable detectors or imaging devices (“cameras”) have been pursued since the 1950s for intraoperative localization of tumors [4-5], because a completeness of the removal of the tumor tissue is critical for the survival of the patient [6-8]. They can detect gamma or beta rays in the close proximity of the radio-labeled tumor, which allows the maximum removal of the malignant tissue while sparing normal tissues for the best trade-off of the patient survival and the quality of life. While the great penetration of γ photons is essential for tomography, this property is disadvantageous for a portable device due to the necessity of heavy metal shielding and collimation, which limit sensitivity, resolution and maneuverability of the probe. More importantly, the γ rays emitted from the tumor site are difficult to be discriminated from those from normal organs, for example metabolic active liver or bladder when using ^{18}F -FDG, since the portable imaging probes generally are not capable of resolving the 3D tracer distribution. Indeed, the γ probes usually use low energy γ emitters (less than 200 KeV) than that used

in PET (511 KeV from positron annihilation). As an alternative, beta cameras have been pursued for smaller size and less interference [9-12] since beta particles (β^+ : positron and β^- : electron) interact continuously with tissues and detector materials and result in a short travel distance [13]. This short range provides a natural shielding and collimation mechanism that can be exploited to develop miniature devices for in situ or subcutaneous imaging. In this work, we aim to study the transportation of beta particles in matter (air and water, where the latter mimics the human soft tissue) through theoretical analysis and Monte Carlo simulations. This study will lay a foundation for the development of high-sensitivity beta detectors, which can be valuable for image-guided therapies of cancer.

1.1 Radiotracer

Radiotracers (radiopharmaceuticals) are combinations of a drug or a biologically active compound which acts as a vehicle for targeted delivery and a radioisotope for localization purposes. The use of radiotracers in nuclear imaging is a non-invasive method for accessing cellular functions, which involves identifying useful biomarkers, specific characteristics of a disease, or biochemical processes that need be measured. Some general properties of a radiotracer are :

- The effective half life of the radiopharmaceutical should be appropriate to serve the imaging purpose and to lessen radiation exposure of the patient. Thus if t_{e1} is the effective half life , t_{b1} is the biological half life and t_{p1} is the physical half life, then

$$\frac{1}{t_{el}} = \frac{1}{t_{pl}} + \frac{1}{t_{bl}} \quad (1.1)$$

- The resulting emission of either γ or beta from the radionuclide should have the proper energy for the detector (e.g. 511 keV for PET and between 100-250 keV for other γ camera imaging devices).
- A high probability of emissions per decay, that is, a sufficient abundance of the signal to be detected.
- A high target to non-target ratio . This helps eliminate most of the background signal and provide more details of the target site. Otherwise it will be almost impossible to distinguish the actual pathology from the background, especially in therapeutic procedures, in order to prevent the patient from excessive radiation dose.
- The radiopharmaceutical should be easily compounded and free of any physiological effect uninterested.
- The radiolabeling should not be affected by the carrier pharmaceutical as this could affect the biodistribution or the compound.

There are several radiotracers used in nuclear imaging today which are specifically chosen to fit both the patient and the test in question. We will focus on two specific radioisotopes F-18 and Cu-64, which are very important and desirable constituents of a vast majority of radiopharmaceuticals today.

^{64}Cu ($T_{1/2} = 12.7$ hours; β^+ , 0.653 MeV [17.8 %]; β^- , 0.579 MeV [38.4 %]) is

generally used as a positron emitter for PET. For example, ^{64}Cu is used as radioisotope in ^{64}Cu -diacetyl-bis(N4-methylthiosemicarbazone)(^{64}Cu -ATSM) especially for the diagnosis of hypoxia. The 12.7-hours half-life of Cu-64, in a practical sense, provide sufficient time for imaging of the target. Due to the versatility of Cu-64, there has been an abundance of novel research in this area over the past 20 years, primarily in the area of PET imaging, but also for the targeted radiotherapy of cancer. Recently, the chelator-free [^{64}Cu]-copper sulfide (CuS) nanoparticles are a good candidate for image-guided photothermal therapy [14,15].

^{18}F ($T_{1/2} = 109.7$ min; β^+ , 0.635MeV [97%]) on the other hand is a major constituent of several radiopharmaceuticals. A Radiotracer like 2-Deoxy-(^{18}F) fluoro-D-glucose (FDG) is the most common radiotracer used in PET to stage cancer and locate metastasis in many regions of the body. FDG is analogous to glucose and is taken up by living cells through the normal glucose pathway. Tumor imaging with FDG relies on the fact that malignant cells show higher metabolic rates of glucose absorption than normal tissue and therefore take up greater amounts of FDG [16-19]. The radionuclide ^{18}F has a high specific activity, and emit positrons with low energy is ideal for PET scans.

1.2 Beta-decay

In a typical beta decay, a radioactive nuclide emits a beta particle (an electron or positron) when a neutron/proton transforms into a proton/neutron (Beta minus, β^- , decay/ Beta plus, β^+ , decay). This means that the atomic number of a parent nuclide will be increased or decreased by one unit, while the mass number remains unchanged. This mode of radioactive decay is of great importance in nuclear medicine and thus constitutes

the crux of this research. The goal of this thesis is to adapt the properties of the emitted β^- and β^+ particles from ^{64}Cu and ^{18}F for a theoretical analysis and simulation using GEANT-4 tool kit.

1.3 Interaction of Beta Particles with matter

To better detect beta radiation in several hundred KeVs range from ^{64}Cu and ^{18}F , it is important to understand how these beta particles interact with matter. Radiation in general deposits energy in matter through a series of ionizations and excitations. Understanding these interactions can provide the fundamental information for the development of portable nuclear imaging devices for efficient detection of beta particles in a feasible range of interest.

A beta particle propagating through matter (depending on its energy) could deposit energy by one of two processes known as: Collisional losses and Radiative losses. More details will be given in Chapter 2.

1.4 Geant4 - Monte Carlo (MC) simulation

There are several MC programs available in nuclear imaging and internal dosimetry with many of them available as open source codes. Current review of those can be found in [20]. There are packages that simulate the transport of radiation through matter such as: PENELOPE [21], GEANT4 [22], MCNP [23] and EGS4 [24]. A number of tools for PET simulation have been developed over the years based on these codes, such as SIMSET [25], PETSIM [26] or EIDOLON [27] which are based on MCNP, and GATE on GEANT4 [28]. A handful of these toolkits are limited by the complexity of the

model, and the computation time required for simulation.

Although the theoretical analysis can give the average distance of beta particles traveling in matter, more detailed information can be acquired using GEANT4-MC simulation. Geant4 (GEometry ANd Tracking -4) is a simulation tool kit for the passage of particles through matter developed by the high energy physics community. Because of its original set of physics processes, modeling content and simulation accuracy, Geant4 toolkit is being used in studies in medical and space sciences as well as nuclear and accelerator physics[29].

Monte Carlo (MC) methods on the other hand, are numerical calculation methods based on random variable sampling. Named “Monte Carlo” by Von Neumann after the most well known center for gambling: The Monte Carlo in Monaco principality[30] because of its similarity to the statistical simulations of the games of chance. The general idea of Monte Carlo analysis is to create a model, which is practically similar to the real physical system of interest, and to create interactions within that system based on known probabilities of occurrence using, whenever suitable, random sampling of Probability Density Functions (PDFs). Virtually, any complex system can in principle be modeled, if the distribution of events that occur in a system is known from experience or other means, and thus a PDF can be generated to simulate the real system.

In Chapter 3, we will use Geant4- MC to simulate the propagation of Beta particles through water (representing human tissue) in detail. The Beta particles with the energy spectrum same as that of ^{64}Cu will be tracked and their scatter patterns will be analyzed using the ROOT software package.

Chapter 2

Beta-decay

In a typical beta decay, a radioactive nuclide emits a beta particle when a neutron/proton transforms into a proton/neutron emitting a beta particle in the process, which could either be an electron or a positron. Beta particles are fast electrons or positrons produced in the weak interaction[31] decay of neutrons or protons in neutron or proton rich nuclei . In a radioactive nuclei with more neutrons than proton, will decay by emitting an electron, an electron neutrino, and convert the neutron into a proton. The decay process could be represented by



on the other hand, nuclei which has more protons than neutrons would decay by emitting a positron, neutrino and convert the proton into a neutron. This decay could be represented by



Alternatively, a third process in with an electron close to the nucleus is captured by a proton is called electron capture which could also be represented as



This processes transforms the nucleus of one atom into another (*nuclear transmutation*), as the daughter nucleus now contains one proton more or less as the case may be.

Energy released in this decay is in fact shared between the beta particle and the neutrino. Contrary to what we expect, there are “no” even sharing (for the most part) of this kinetic energy between both ejected particles during this process, rather the sharing is random between decays. This random sharing of energy between both particles gives the electron(beta particle, which is detectable) a kind of spectrum or energy distribution, for a nuclide decaying by the emission of β^- . Thus having a maximum possible energy of for each decay and distribution that also shows the minimum energy available. This thus, gives a unique signature to every beta emission from every radioactive nuclide.

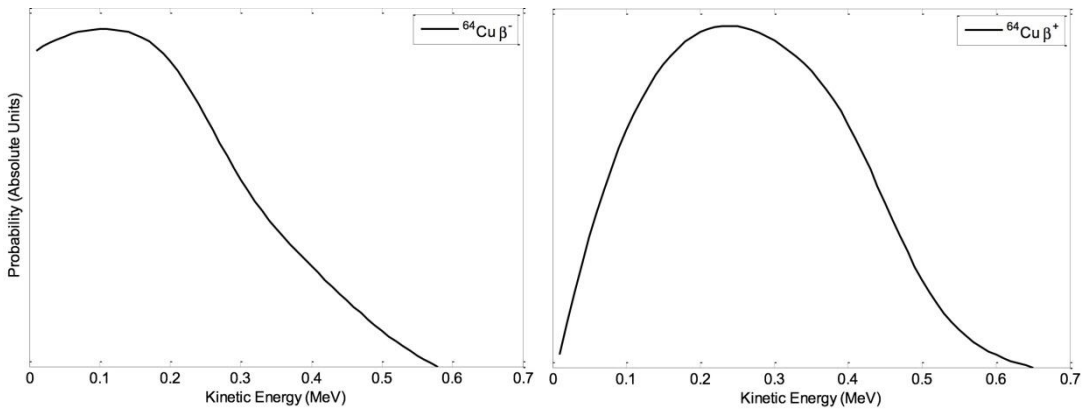


Fig 2-1 β^- spectra obtained from decaying Cu -64. β^- particles are affected by the electric field of the positively charged nuclei and thus the energy spectrum is shifted towards lower energies. β^+ particles, on the other hand, are repelled by the nuclei so the energy spectrum it is shifted towards higher energies [32].

2.1.1 Interaction of beta particles with matter

As ionizing radiation propagates through matter, it interacts and losses energy via

several mechanisms. To detect such radiation, we look for the unique feature of the interaction and the amount of energy deposited in the material. In nuclear medicine these materials are either detectors or absorbing medium (human tissue). Thus one needs to know how radiation interacts and what the consequences are of the various interactions [4]. In this work we focus only on Beta interactions with matter particularly their interactions with select materials and elements such as air, water, Kapton, berillium(Be), copper (Cu), and iron (Fe). These elements and materials constitute both the medium (air and water mimicking human tissue) and detector components (Be, Cu, Fe). Consequently, a radiation detector depends on the manner in which the radiation to be detected interacts with the material of the detector itself.

Beta particles at low kinetic energy interact with a medium primarily through the long range Coulomb force with the orbital electrons and the nucleus[27]. When beta particles interact with a medium they loose energy and are brought to rest after transversing a finite distance called *range*. The range depends on the type and energy of the incoming beta particle and the material it is transversing[4]. Depending on the proximity of the incoming beta particle to the atom of the medium, this interaction could lead to either cause an excitation or ionization of the atom. Ionization occurs when the incident beta particle interacts closely to an orbital electron with energies greater than the electron binding energy, knocking it out of the atom completely and thus ionizing the atom. On the other hand, when the incoming beta particle interacts from a distance with just enough energy to raise an orbital electron to a higher shell the atom becomes excited. Collisions (interactions) that result to ionization or excitation are called *inelastic collisions*. Classically, these interactions can be divided into three categories depending

on the impact parameter b compared to the atomic radius a :

1. Interaction of the charged particle with the external nuclear field (bremsstrahlung production) for $b \ll a$.

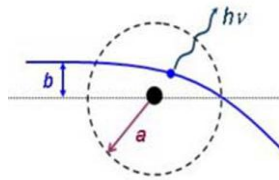


Fig 2-2 A Radiation collision between a charged particle and an atom for $b \ll a$ [33].

2. Interaction of the charged particle with orbital electron for $b \approx a$.

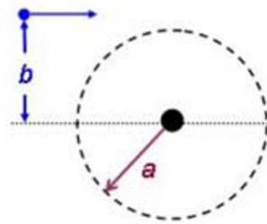


Fig 2-3 A hard collision between a charged particle and an atom for $b \approx a$ [33] this would ionize the atom .

3. Interaction of the charged particle with orbital electron for $b \gg a$.

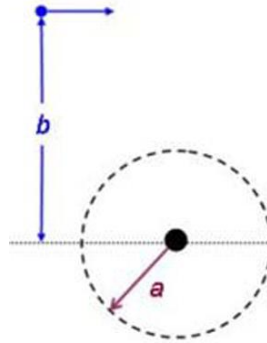


Fig 2-4 A soft collision between a charged particle and an atom for $b \gg a$.
In this case the atom would be in an excited state afterwards[33].

The collisions between the incident beta particle and the orbital electron or the nucleus of an atom may be either elastic or inelastic. In the elastic collision the beta particle is deflected from its original path without any loss of energy, while in the inelastic collision, beta particles are deflected with a loss in its energy. This lost energy is transferred to the orbital electron or could be emitted in form of bremsstrahlung. Beta particles do have a large number of interactions before they exhaust their kinetic energy in a medium. Since the mass of a beta particle is approximately same as that of the orbital electron each interaction could cause a change in the path of the incident beta particle. The results is an elastic or inelastic scattering in which a beta particle loses a greater fraction of its energy from one of such scattering[34].

There are two mechanisms by which beta particles deposit energy in matter, these are:

- A. Collisional losses
- B. Radiative losses

A. Collisional Losses.

This is the result of interaction between a fast moving beta particle and an orbital electron in a medium. It could cause excitations or ionization of the atoms in the medium. Ionization loss by electrons and positrons differ somewhat, especially in heavy particles because of the spin, and kinematics of the incident beta particle with the electrons which it ionizes.

At low energy, energy transfer from the beta particle to matter in each individual atomic interaction is generally small, so that the particle has to undergo a large number of interactions before it comes to rest. Large scattering angles would be expected during collisions since the particles involved are of the same mass. In some collisions, beta particles could be bounced back from the same surface or direction they entered into the medium. This phenomenon is called *backscattering*.

Backscattered beta particles do not deposit all their energy in the medium, and therefore they constitute a significant flaw in the response of the detector which has been designed to collect electron energy spectra. Beta particles with high incident energy and absorbers with low atomic number have the lowest probability for the backscattering effect[25]. The effect is particularly strong for beta particles with low energy, and increases with the atomic number Z of the material. Backscattering also depends on the geometry, energy and incidence angle of the beta particles. In detectors for instance, a large fraction of electrons may be scattered out before being able to produce a usable signal.

B. Radiative losses

This occurs when a beta particle passing a nucleus is deflected by the Coulomb

field of the nucleus and it emits a bremsstrahlung radiation. The emitted radiation has a continuous energy distribution from zero to a maximum kinetic energy of the incoming electron.

2.1.2 Stopping power

Stopping power is a parameter used to describe the gradual loss of energy of the charged particle (beta particle) as it propagates in a medium. There are two classes of stopping powers known as: collision stopping power and radiative stopping power. As the names imply, collision stopping power is the consequence of an incident particle interacting with orbital electrons of the medium while radiative stopping power, results from interaction with nuclei of the medium. This parameter is dependent on the properties of the Beta particle such as charge, velocity, energy and mass as well as on the properties of the propagating medium such as its density and atomic number.

For beta particles, energy transfers due to soft collisions are combined with those due to hard collisions using the Møller (for electrons) and Bhabba (for positrons) cross sections for Beta particles[33]. For beta particles in a given medium of density ρ the mass collision stopping power is given by

$$S_c = 2\pi r_e^2 \frac{Z}{A} N_A \frac{m_e c^2}{\beta^2} \left(\ln E_k - \ln I + \ln \left(1 + \frac{\tau}{2} \right) + F^\pm(\tau) - \delta \right) = \frac{1}{\rho} \frac{dE}{dx} \quad (2.0)$$

where :

E_k is the kinetic energy of the incoming beta particle

F^+ stopping power function for positrons

F^- stopping power function for electrons

N_A Avogadro's number (6.022×10^{23} atom/gram-atom)

- Z Atomic number
- A Mass number of absorbing media
- I Mean ionisation/excitation potential
- m_e electron rest mass (0.511 MeV / c^2)
- r_e classical electron radius (2.818 fm)
- β normalized particle velocity (v/c)
- δ density effect correction for stopping power
- τ normalized electron kinetic energy ($E_K / m_e c^2$)

and the functions $F(\tau)$ is given by:

$$F^-(\tau) = (1 - \beta^2) \left(1 + \frac{\tau^2}{8} - (2\tau + 1) \ln 2 \right) \text{ for electrons} \quad (2.1)$$

$$F^+(\tau) = 2 \ln 2 - \left(\frac{\beta^2}{12} \right) \left(23 + \frac{14}{(\tau+2)^2} + \frac{4}{(\tau+2)^3} \right) \text{ for positrons} \quad (2.2)$$

(dE/dx) The rate of energy loss per unit of path length by a charged particle in a medium is called the linear stopping power

The stopping power is typically given in units MeV · cm² /g and then referred to as the mass stopping power S equal to the linear stopping power divided by the density ρ of the absorbing medium.

In addition to stopping powers, other parameters of charged particle interaction with matter, such as the range, energy transfer, mean ionization potential, and radiation yield are considerably as important in nuclear imaging and radiation dosimetry.

2.2 Transportation of Beta Particles

Like any other radiation traveling in matter, the range, energy deposited, and scattering patterns are very important properties in nuclear medicine. The range of a beta particle in specific material could be defined as the total distance traveled by the beta particle after a continuous loss of its initial energy and is brought to rest in the material. This distance must be a well defined number, the same for all identical particles with the same initial energy in the same type of material. This quantity depends on the type of material, the particle type and its energy. Although, energy loss is not continuous, but statistical in nature, experiments show that identical particles exhibit a statistical distribution of ranges about some mean value. For beta particles propagating through a media at low kinetic energy, relativistic effects become important. Moreover, Collisions with orbital electrons may result in large energy transfers of up to 50% of the incident electron kinetic energy[33], while collisions with nuclei of the absorber may result in bremsstrahlung production (radiative loss).

Range energy relation is necessary for deciding the sizes of detectors to be used in an experiment or in determining the thickness of radiation shielding.

2.3 Detection of beta particles

Because certain materials/substances exhibit significant glow or ionizations when a beta particle travels through them, They used as detector materials for detecting beta particles. One class of detectors employs gas as the detection material. Ionization chambers, proportional counters, and Geiger-Müller counters are of this class. In these detectors, after entering through a thin window, the beta particles produce positive ions and free electrons as they collide with atoms of the gas in the process of their slowing

down. An electric field applied across the volume of gas causes these ions and electrons to drift along the field lines, causing an ionization current that is then processed in external electronic devices[35].

2.3.1 Detection of Beta particles by GEM detectors

The Gas Electron Multiplier (GEM) is a technology for gaseous detector introduced by F. Sauli in 1996, at CERN [36]. Various developments have been made to improve the GEM detectors over the years. They are based on the use perforated plastic plates (thin kapton foils of about 50um) coated on both sides with metallic or resistive coating (copper of about 5um) .

The perforations are usually double-conical, with an inner radius of 50um and an outer one of 70um, disposed on a hexagonal grid of 140um pitch. Applying a moderate difference of potential (100V) between the two conductive sides of the GEM, a strong electric field (10kV/cm) is created at the center of the holes, where the field lines are focused initiating an avalanche: part is collected on the bottom side of the GEM, and the rest of the electrons drift towards the read-out anode - or the next amplification stage, in a multiple GEM-stack. A unique feature of this technology is the ability to put several GEMs in cascade to reach multiple amplification factors of over 10^6 [37].

This work provides the necessary information on the distribution of beta particles in the various components of the GEM detectors for the construction of clinical and preclinical imaging devices, based on the information from emissions from Cu-64 radiopharmaceuticals. The high spatial and energy resolution of the GEM detectors will make it possible to distinguish different radio-markers in small volumes and are very useful in detecting very low radiation levels as well as in single photon counting mode.

2.3.2 Detection of Beta particles by scintillators.

Scintillators are materials (solids, liquids or gases) that produce sparks or scintillations of light when ionizing radiation passes through them[29]. The passage of a charged particle through matter could temporarily raise electrons in the material into excited states. When these electrons fall back into their normal state, light may be emitted and detected as in the scintillation detector the amount of light produced in the scintillator is very small. It must be amplified before it can be recorded as a pulse. The amplification or multiplication of the scintillator's light is achieved with a device known as the photomultiplier tube (PMT). A PMT accepts a small amount of light, amplifies it many times, and delivers a strong pulse at its output. Scintillators could be made of either inorganic crystals or organic compounds.

2.3.2.1 Inorganic scintillators.

Inorganic scintillators rely on the crystalline nature of the material for light production and most have impurity atoms, with ionization potentials less than atoms of the crystal, added as activators. Photoelectric absorption or Compton scattering in the crystal leads to scintillation light that is usually converted to an electrical pulse by a photomultiplier tube. Ionizing radiation may elevate electrons from the conduction band to the valence band of the crystal. The electrons can migrate in the conduction band and holes left in the valence band may also move and ionize a host atom that it encounters. The impurity ions introduce trapping levels in the energy gap between the valence and conduction bands.

2.3.2.2 Organic (plastic) scintillators.

Organic detectors are low energy resolution detectors. They are useful for

detecting a variety of radiation especially in coincidence systems where a particle or gamma-ray loses a small part of its energy to the detector. Among all the detectors, plastic scintillators exhibit very short response time and are extensively used for experiments where accurate measurements of very short time intervals at the level of nanosecond must be obtained. Other common applications of Plastic scintillators offer high performance, ease of handling, and mechanical stability at a relatively lower cost when compared to inorganic scintillators such as NaI, CsI or LaBr crystals

2.3.3 Detection of Beta particles by solid state detectors

In a semiconductor detector, a solid media replaces the gas. When a beta particle enters the detector, it causes struck electrons to be raised into the conduction band, leaving holes behind in the valence band. The electrons and holes move under the influence of an imposed electric field, causing a pulse of current to flow. Such detectors are useful mainly for low-energy beta particles. A less obvious but fundamental advantage of semiconductor detectors is the fact that much less energy is required ($\sim 3\text{eV}$) to produce a hole-electron pair than that required ($\sim 30\text{ eV}$) to produce an ion electron pair in gases [34].

These detectors offer by far, the best spectral-resolution. Their high-resolution is especially important in the identification of the isotopic composition of the source of radiation and in the ability to detect a source in the presence of background. Most promising of these detectors are those based on the CdTe or CdZnTe. These materials have, until recently, been available in only small volumes ($\sim \text{few cm}^3$) but they do have the advantage of being able to provide a spectral-resolution some 30-40% better than

LaBr 3 . These detectors will not play a significant role when a large volume detector is required because of their small size and modest stopping power.

Chapter 3

Monte Carlo simulations

A MC simulation is a model that simulates the behavior of a system, based on a priori knowledge of the probabilities of occurrence of the different processes or interactions that determine the desired outcome. They are useful resort to study the interaction of radiation with matter [38,39]. Considering the stochastic nature of radiation emission and detection processes, MC method is of particular interest for medical physics especially in areas such as radiotherapy, radiation protection and nuclear medicine [40]. Today, simulation techniques have become an essential research tool in nuclear medicine for the study of the response of imaging systems, like PET and SPECT scanners, predicting the performance of new detectors and optimizing their design [41,42]. Hence, data obtained from MC simulations are essential in the development, validation and evaluation of medical image reconstruction techniques and for the assessment of correction methods. One of the advantages of MC simulations is the possibility to change different parameters and to investigate the effects of such modifications on the performance of scanners, allowing testing several detection configurations that may be impossible or impractical in an actual experiment.

This work investigates the transportation of Beta particles through water, air, and a GEM detector using the GEANT4-MC tool kit. First the tracks and energy deposit of beta particles in the the various components of a GEM unit are considered separately. The GEM unit is intended to detect beta-particles in a mixed beta/gamma radiation fields. The detection efficiency of the unit and the position dependence of the beta particles is also simulated in this chapter.

3.1 Method and Simulation procedures

3.1.1 Installation of GEANT4 Simulation packages

As a requirement for the installation of GEANT4 package the operating system/platform on which the user intends to use this tool has to be compatible with the tool kit. At the time of this simulation our operating system (Ubuntu 15.04) was not officially supported by Geant4 group at CERN. This pose a great challenge as there were many problems encountered during the installation of the tool kit that were not easy to figure out. Thus a lot of time was spent trying to figure out these problems.

While installing GEANT4, there are several other softwares are needed to build and install Geant4. These packages work hand in hand with the toolkit, and also serve as external sources for several other functions in Geant4. They include:

- CMake 3.1.1 (for this work)
- C++ Compiler
- CLHEP Libraries
- X11 OpenGL.(for visualization)

The Geant4 source code could be obtained from the Geant4 web site and installed after the above listed packages have been successfully installed. Part of the building and installation procedures involved, choosing what DFLAGS to turn ON/OFF.

3.1.2 Considerations for simulation

In nuclear medicine, the patient is administered a radio pharmaceutical that distributes according to a specific physiological or functional pathway. The patient is then imaged using external radiation detectors to determine the in vivo distribution and dynamics of the radiopharmaceutical through which the patient's physiology can be

inferred. This means two things for our simulations, first that the source of radiation has to be immersed in the material (tissue) and secondly, our source must have specific energy for a given beta decay process. Our target materials are shown in the table below.

Table 3-1 Elements and their composition/properties considered for this simulations.

Element/ substance	Composition	Atomic number	density	Mean excitation energy
Water	H, O	1 , 8	1 g/cm ³	75 eV
Beryllium	--	4	1.848 g/cm ³	63.7 eV
Iron	--	26	7.874 g/cm ³	286 eV
Air	C, N,O,Ar	6,7,8,18	0.00120479 g/cm ³	85.7 eV
Kapton	H,C,N,O	1,6,7,8	0.209235 g/cm ³	79.6 eV

Air and water are chosen in this case to represent the human tissue (60% of the human body: Blood 92%, Brain and muscles about 75% and bones about 22%). Beryllium, Kapton and iron are considered for future work to be done on building a GEM detector for detecting beta particles emitted from our chosen radioisotope.

Radiopharmaceutical like F18-fluorodeoxyglucose (FDG) and ⁶⁴Cu – ATSM (diacetyl-bis(N4-methylthiosemicarbazone)) have ¹⁸F and ⁶⁴Cu as their source radioisotope. These two radioisotopes are our target element as both decay by emitting beta particles. Table 3-2 shows the decay properties of both radioisotope for our experiment.

Table 3-2 Decay properties of Cu considered for simulation.

Element	β^-	β^+	Half life(hr)	Energy KeV (β^-)	Energy KeV (β^+)
^{64}Cu	39%	61%	12.69	579.353	652.834

3.1.3 Simulation set-up and Method

Two blocks were constructed with one encapsulating the other. The outermost block (Purple) which measures 1cm x 1cm x 1 cm represent the boundaries of the simulation while the smaller block (red) is the actual simulation environment(measuring 0.9 cm x 0.9 cm x 0.9 cm). The inner block was made sensitive with a particle source placed at the center (0,0,0). The particle source at the center of the sensitive block were set to reproduce beta particles with the same properties as those emitted by ^{64}Cu and ^{18}F as shown in the table above

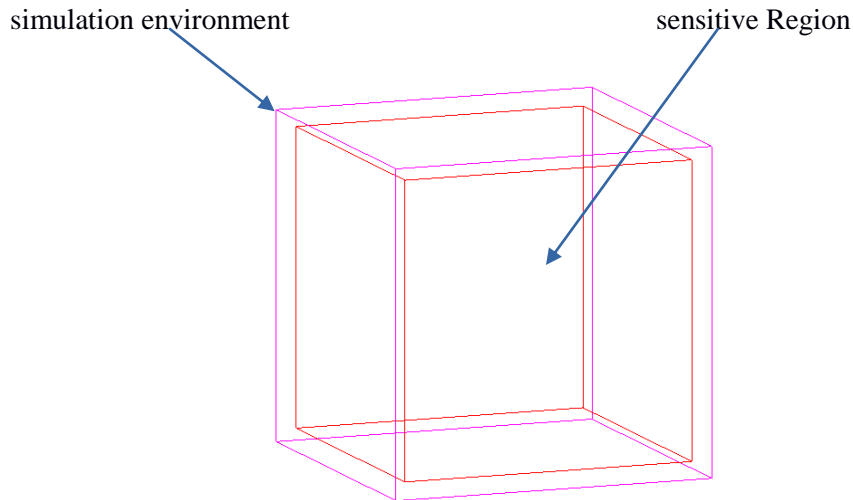


Fig 3.1 Simulation environment showing the sensitive detector (red).

Various materials to be used were defined using “G4NistManager” such that any user could select what material from the table to fill in the sensitive region. When filled with

water, and the appropriate particle source energy is chosen, the above set up would represent a human tissue as a source of radiation.

3.2 Results

3.2.1 Beta Particles in Air.

The results presented below was generated by 193 electrons at 579 KeV and 88 positron beams at 653 KeV. The various events were collected in steps of 0.05 mm from the source at the center of the simulation environment. Fig 3-2 and 3-8 show mostly electrons and positron activities. There was no ionisation or γ photons released as beta particles traveled in air. Furthermore, Fig3-3 to Fig 3-5 as well as Fig 3-9 to Fig 3-11 shows the range of beta particles in air. In both cases (electrons and positrons) beta particles traveled outside the range of our simulation environment, thus no conclusion on the range could be done for air.

Fig 3-6 shows how much energy is deposited by the generated particles in air. Here we see that both electrons and positrons did not lose/deposit energy in air, within our simulation environment. This is further confirmed by figures 3-7 and 3-12 which is a plot of the kinetic energies(KE) of beta particles at various depths in air. For this the KE was plot against the radial distance from the origin.

A. Electrons:

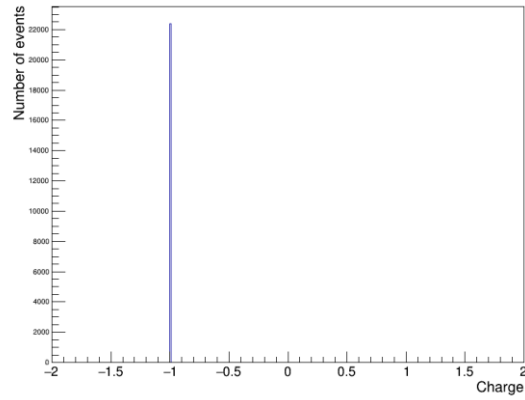


Fig. 3-2 Over 22000 events all of which were registered as electrons.

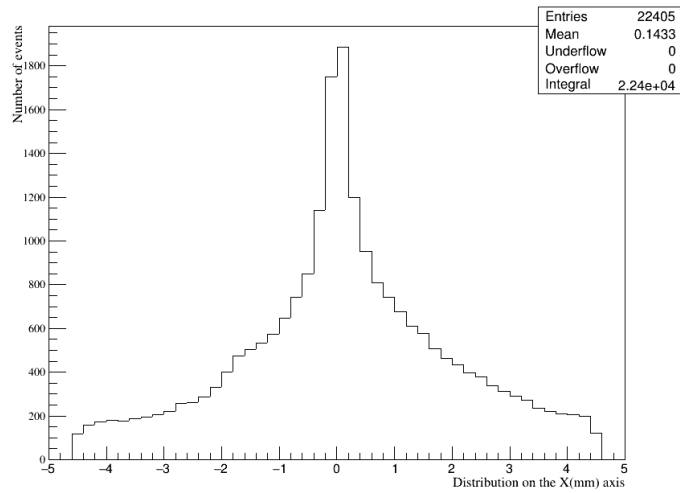


Fig 3-3. The displacement of electrons from the origin along the X(mm) axis. the sharp drop shows that the electrons traveled outside the range of our simulation environment.

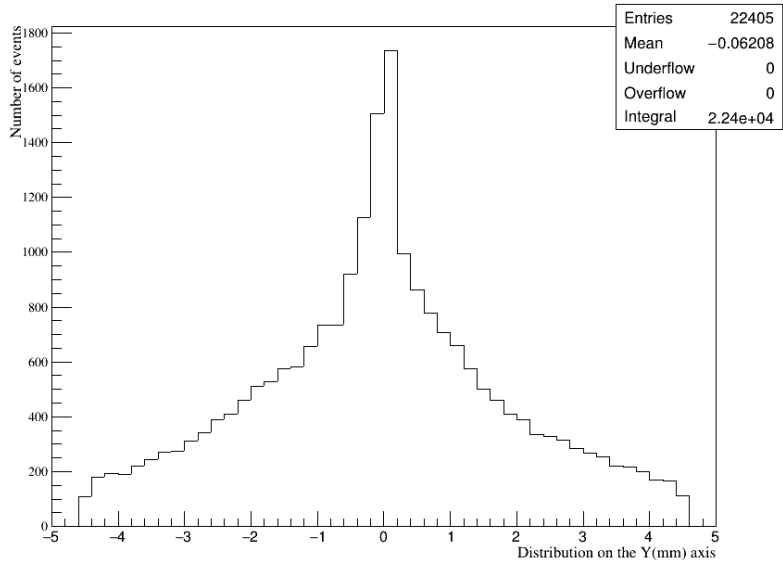


Fig 3-4 The displacement of electrons from the origin along the Y(mm) axis.

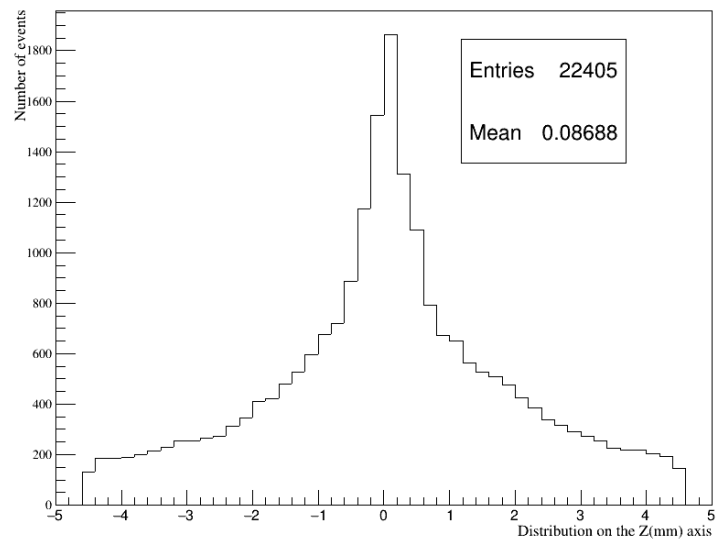


Fig 3-5. The displacement of electrons from the origin along the Z(mm) axis.

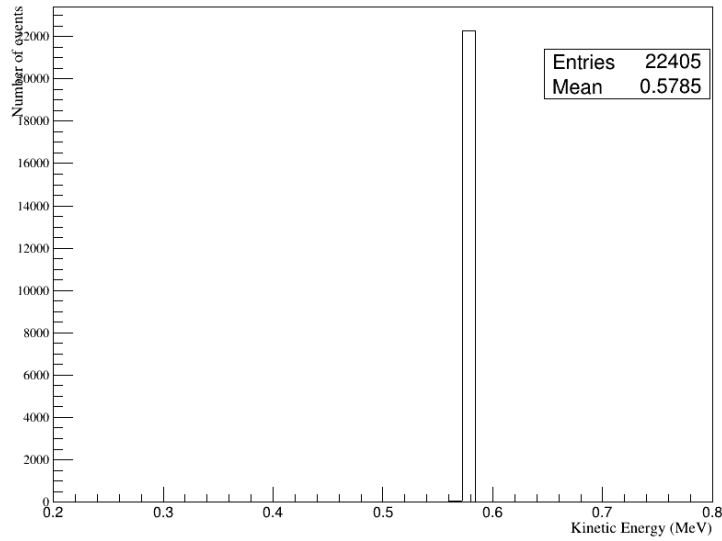


Fig 3-6 The kinetic energy of electron events within the simulation environment showing most events still had about 579 KeV energy outside the range of our simulation.

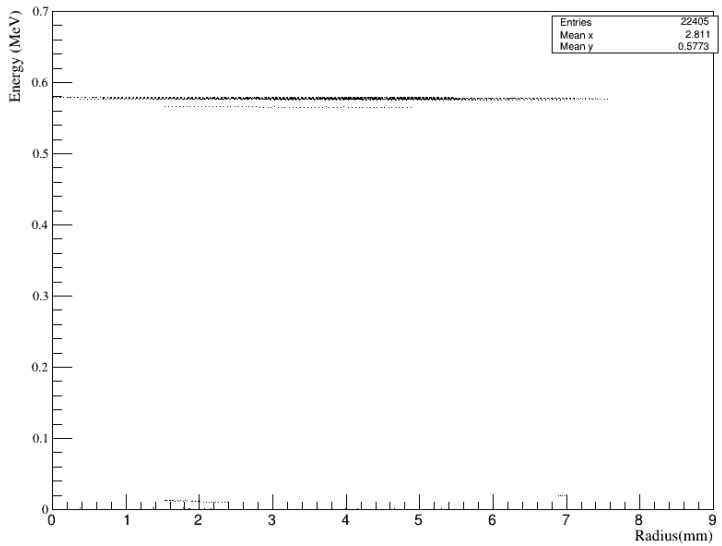


Fig 3-7 Energy vs radial distance traveled by electron in air. Again most events escape the simulation environment with little or no loss in energy.

B. Positrons

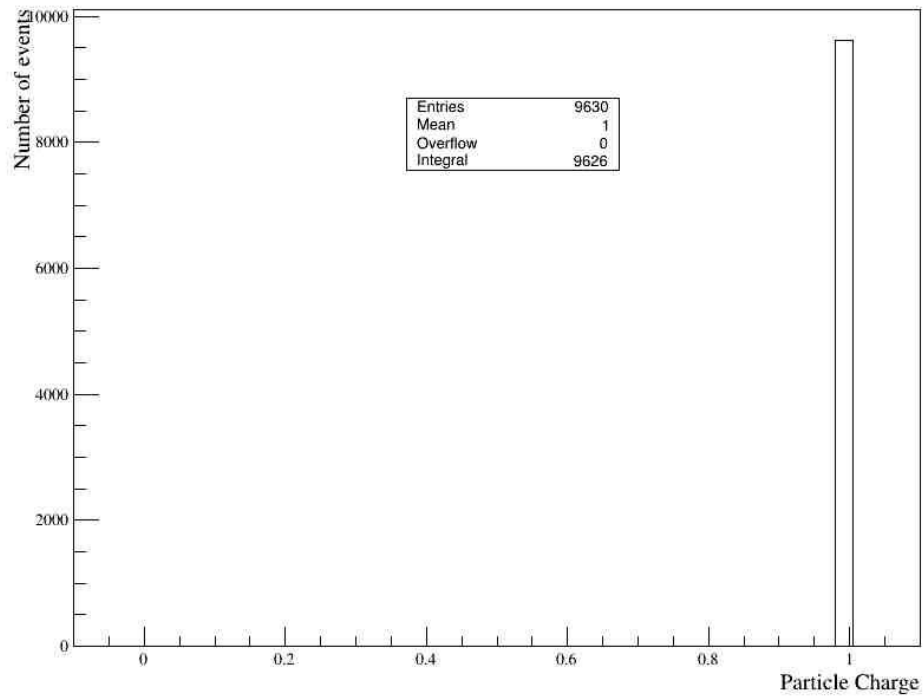


Fig 3-8. Number of events registered as positrons within the simulation environment (charge 1).

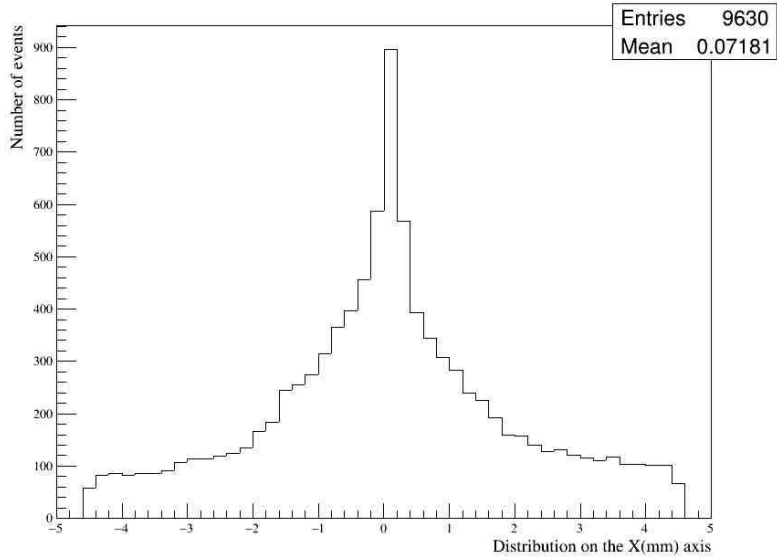


Fig 3-9 The distribution of positrons along the X (mm) axis. Again the sharp drop on the sides show that the positron continued propagation even outside our simulation environment.

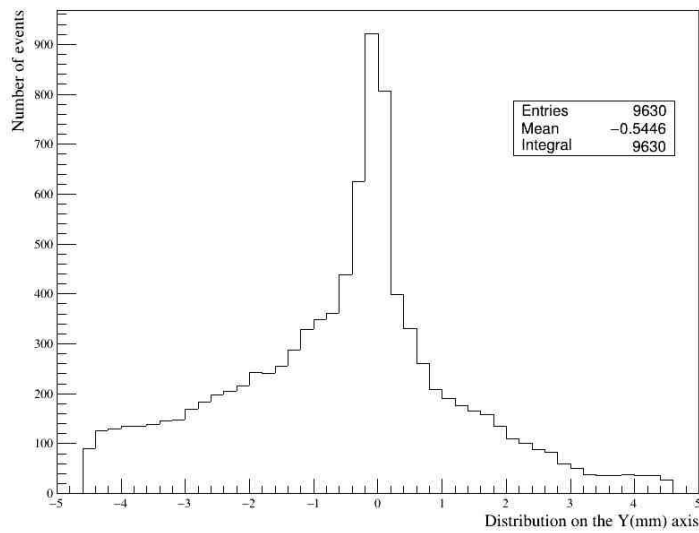


Fig 3-10 The distribution of positrons along the Y (mm) axis.

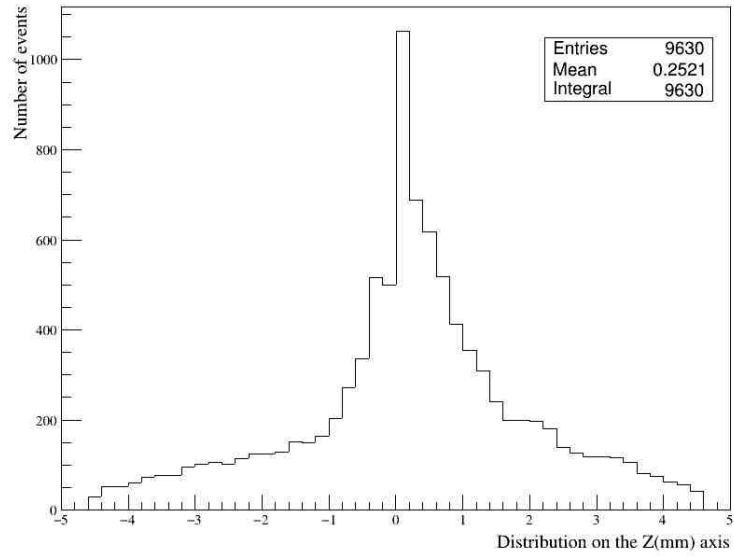


Fig 3-11 The distribution of positrons along the Z (mm) axis.

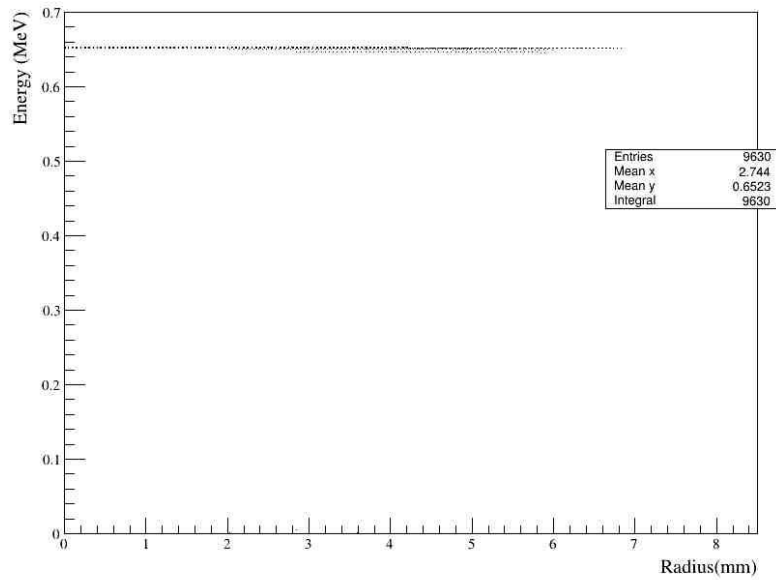


Fig 3-12 Kinetic energy of positron vs radial distance traveled in air within the simulation environment.

3.2.2 Beta particles in water

Below, Fig 3-13 shows primary electron events in water (charge -1). This may include ionization electrons. Fig 3.14 shows bremsstrahlung (about 10 events). Fig 3-21 on the other hand is a mixed field. Here we see, a mixed field comprising of ionisation electrons, annihilation γ photons and positrons. Its difficult to measure or detect beta particles in such fields as the background would significantly interfere. figures 3-15 to 3-17 shows the range of electrons in water (maximum 2.0 mm) while figures 3-23 to 3-25 shows the range of positrons in water (about 2.2 mm) . The 0.2 mm difference is due to the slight difference in the energies of the beta particles. Here again we see both electrons and positrons having very similar behavior in water. Fig 3-18 and Fig 3-26 shows the amount of energy deposited by electrons and positrons in water as they pass through.

The KE of these beta particles at various depths in water are shown in figures 3-19 and 3-28. At zero KE the most energetic electron would have traveled about 2.4mm in water while positrons go as far as 2.6mm. Again this is due to the difference in energy of both beams. These KE is lost in water as a result of collisions with water molecules, figures 3-20 and 3-27 show the 2D projection of beta particle tracks on the XY plane. Some tracks reveal almost a complete deflection of the incoming beta particles as a result of collision.

A. Electrons

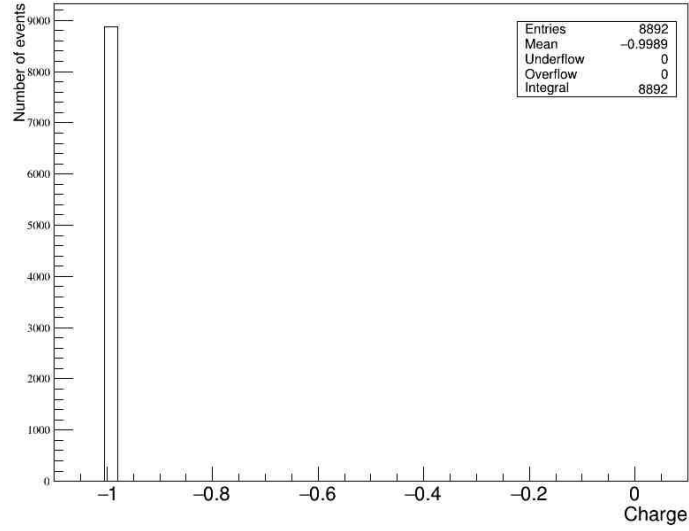


Fig 3-13 Number of events with charge -1 (electrons) in water.

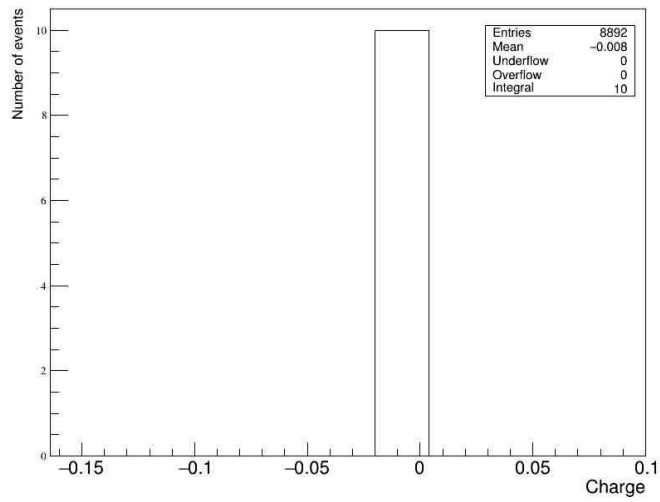


Fig 3-14 A blow up of Fig 3.13 around the origin, showing 10 events of bremsstrahlung radiation.

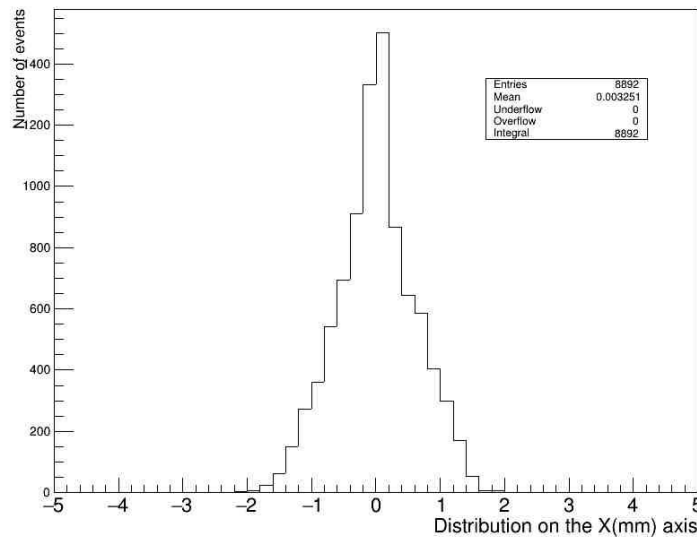


Fig 3-15 Distribution of electrons about the origin along the X axis in water.

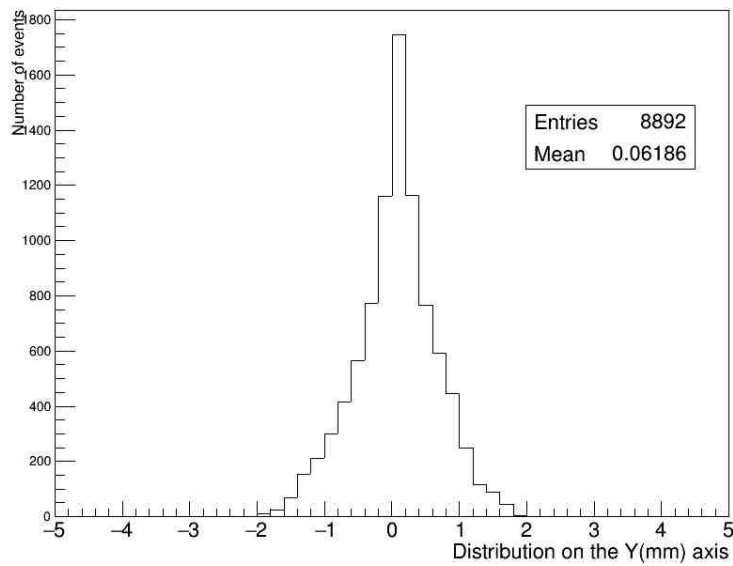


Fig 3-16 Distribution of electrons about the origin along the Y axis in water. here we see the electrons travel approximately 1.8 mm in water.

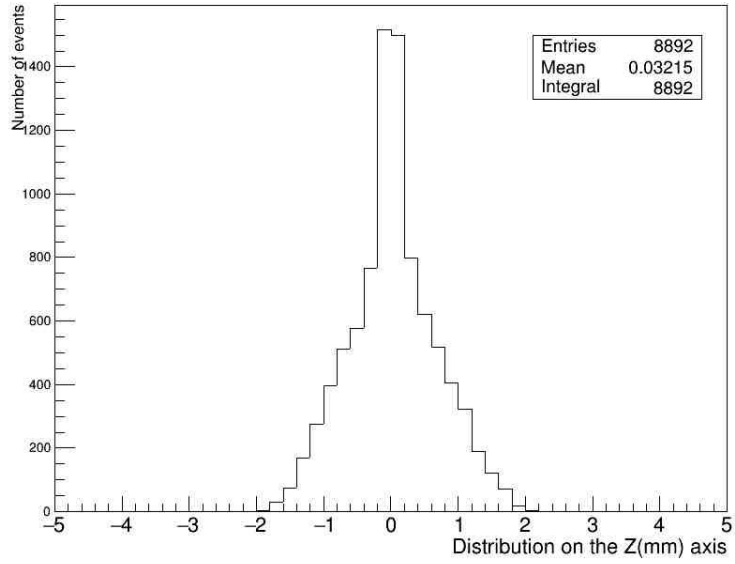


Fig 3-17 Distribution of electrons about the origin along the Z axis in water. Range of electrons is approximately 2.0 mm in water.

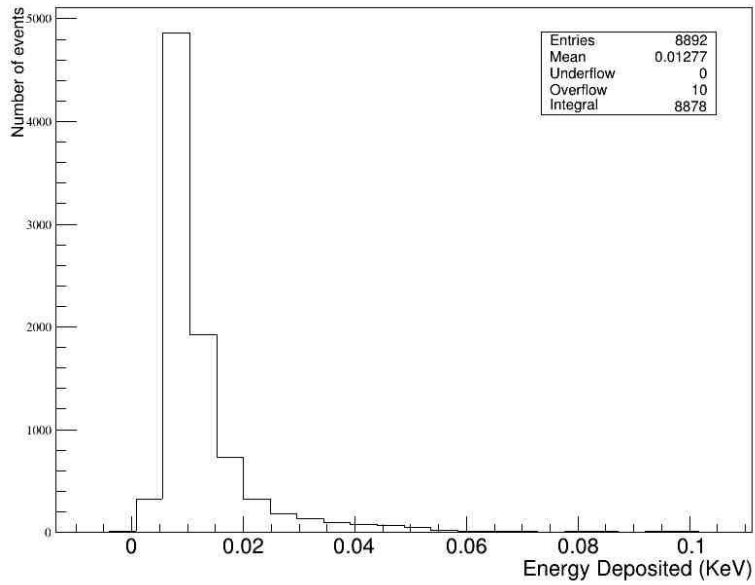


Fig 3.18 Energy deposited in water by electrons.

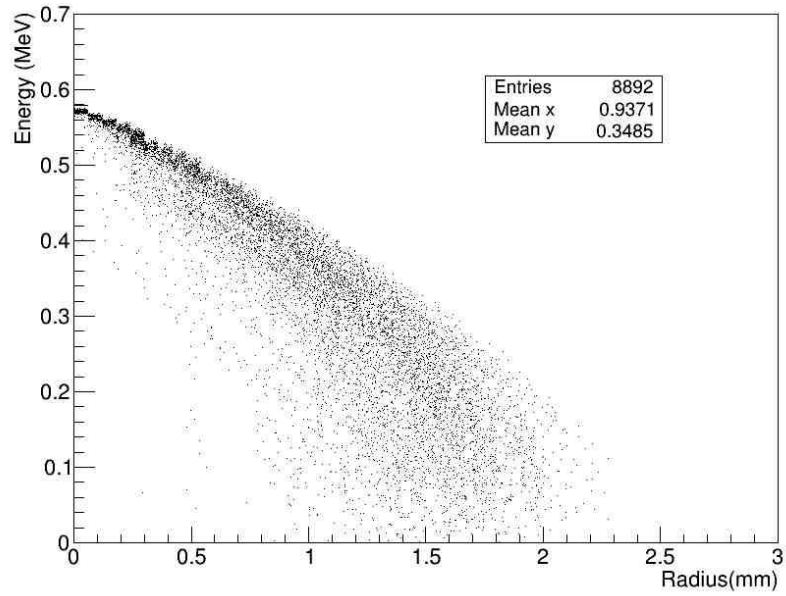


Fig 3-19 Kinetic energy of electrons in water at various depths.

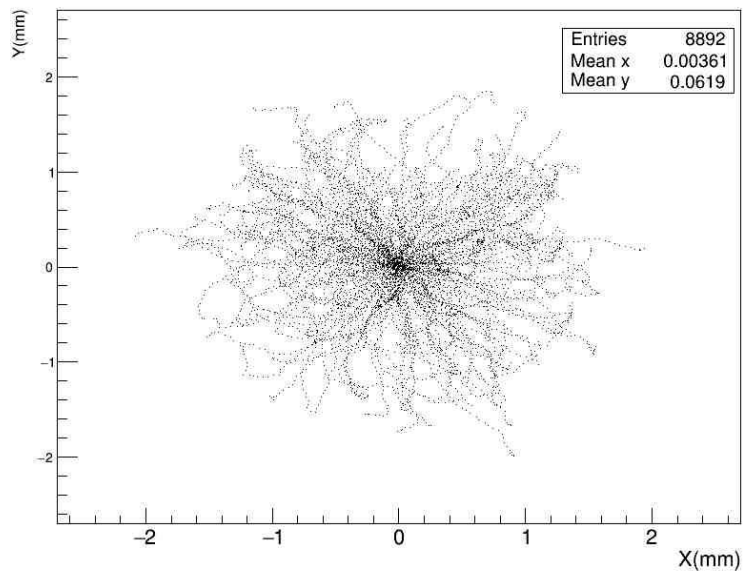


Fig 3-20 Tracks of 579 KeV electrons projected on the XY plane.

B. Positrons

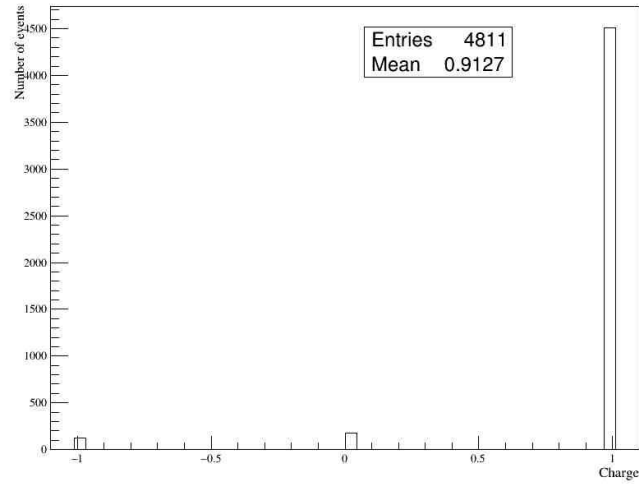


Fig 3-21 Shows a mixed field. Though there are more positron events (about 4500) than there are electrons. The plot also shows that there are gamma photons generated from annihilation processes.

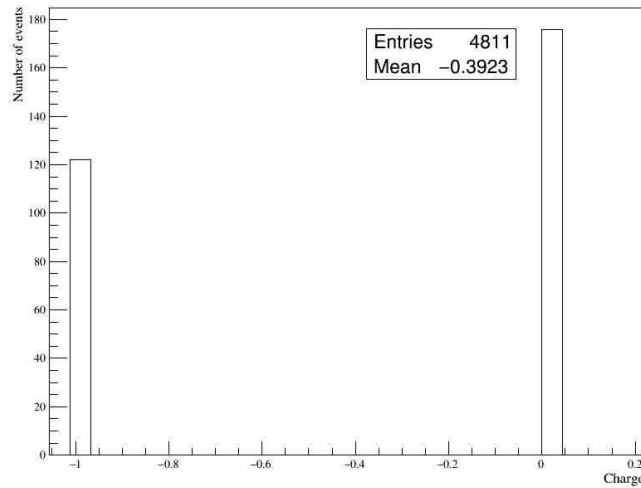


Fig 3-22 Closer look at Fig. 3-20. showing about 180 gamma photons emitted from annihilation processes and about 120 events of ionization electrons.

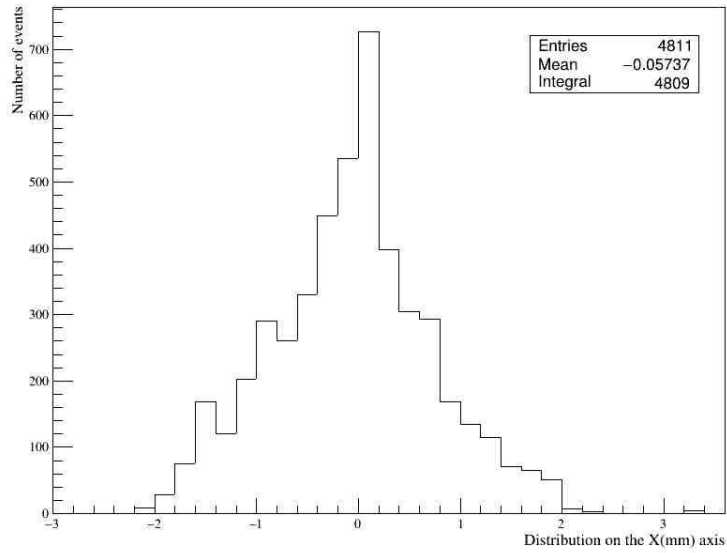


Fig 3-23 Distribution of Positrons along the X axis with a range of about 2.2mm.

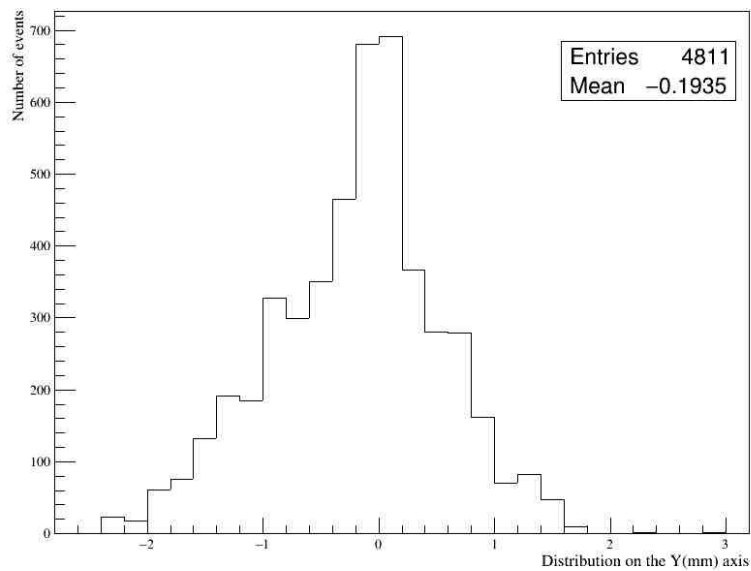


Fig 3-24 Distribution of Positrons along the Y axis with a range of about 1.8 mm.

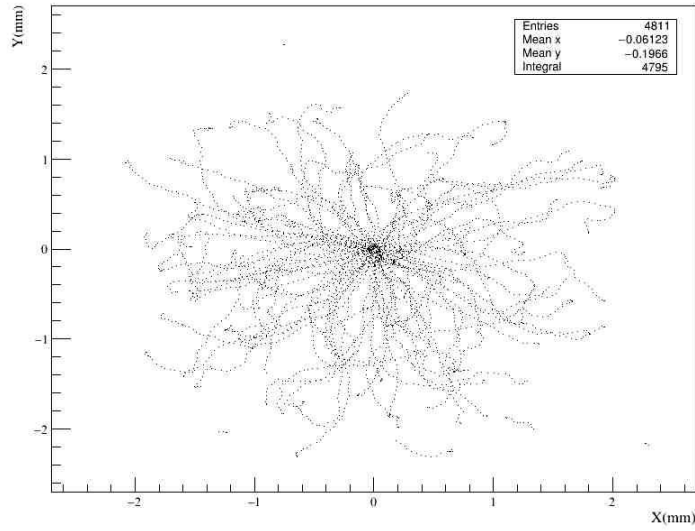


Fig 3-25 Distribution of Positrons along the Z axis with a range of about 2.2mm.

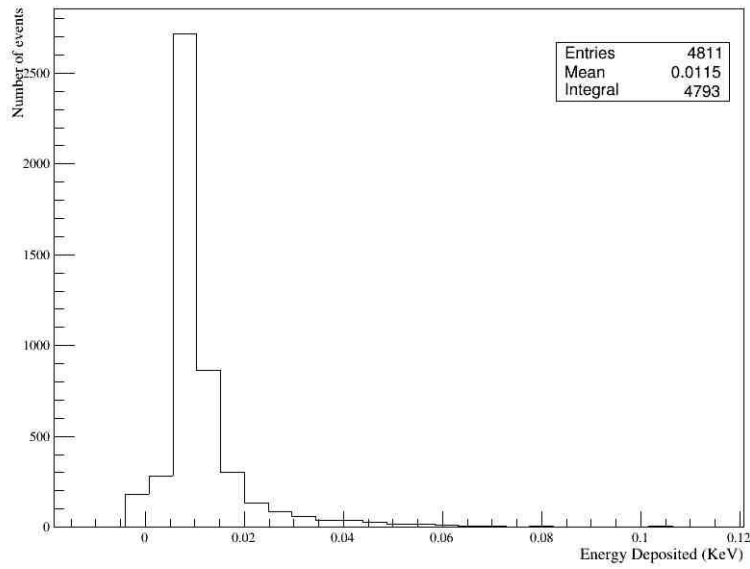


Fig 3-26 Number of events and corresponding Energy deposited in water.

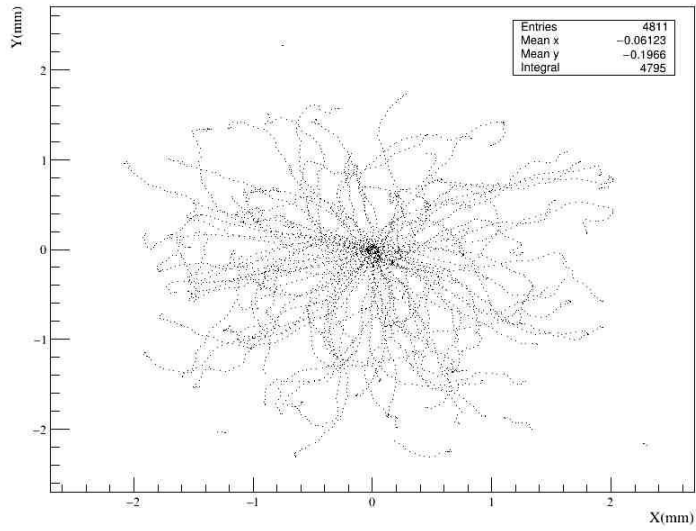


Fig 3-27 Tracks of 653 KeV positrons projected on the XY plane.

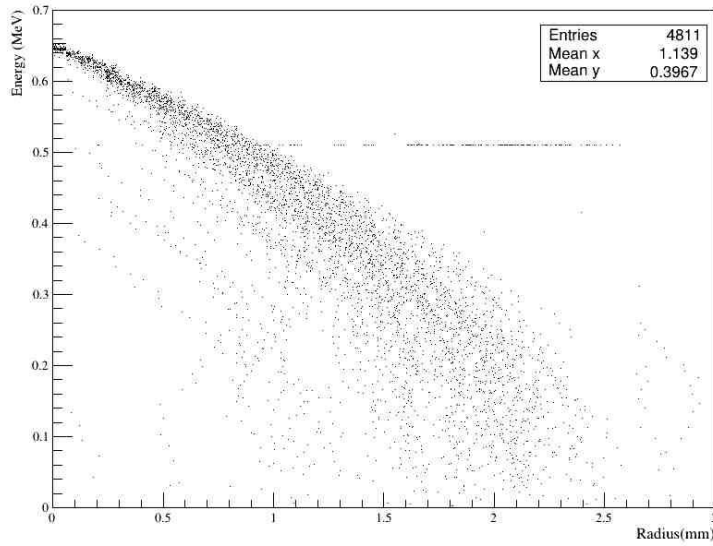


Fig 3-28 Kinetic energy of Positrons at various depth in water. Most energetic particle was brought to rest at about 2.5mm.

3.2.3 Beta particles in Beryllium

In Fig 3-29 below, there are over 500 events of both primary and secondary electrons (initial energy 579 KeV) which generated some secondary γ photons possibly from bremsstrahlung events. On the other hand, Fig 3-38 shows positron events with secondary electrons, from ionization. Figures 3-31 to 3-33 as well as figures 3-39 to 3-41 shows the range of beta particles (electrons and positrons respectively) in beryllium. The range for the electrons is about 1.4mm while positrons travel about 1.8mm. Fig 3-34 and Fig 3-42 shows the energy deposited in beryllium by all the various activities. This is further clarified in Fig 3-36 and Fig 3-43 which is a plot of the kinetic energy of beta particles at different depths in beryllium. Electrons of 579 KeV would loose all of its energy at about 1.55mm in beryllium while positrons at 653 KeV would do like wise in about 1.75mm.

Finally the XY plane projection of the tracks of beta particles in beryllium are shown in Fig 3-35 and Fig 3- 44 for electrons and positrons respectively. The tracks in Fig 3-35 appear darker than those in Fig 3-44 possibly because of the number of beams involved(193 electrons and 88 positrons). But over all we see in both cases that the incoming beta particle is scattered through various angles. The paths also show collisions that led to back scattering and curved tracks.

A. Electrons

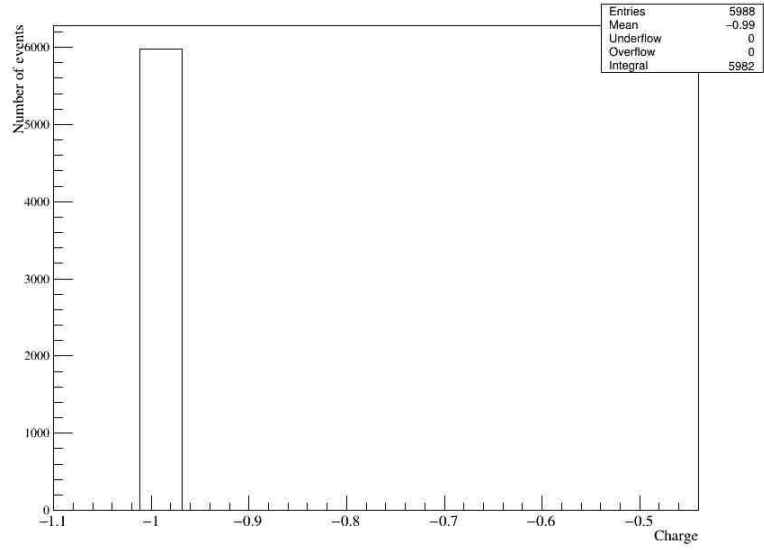


Fig 3-29 Number of events with charge (-1) in beryllium.

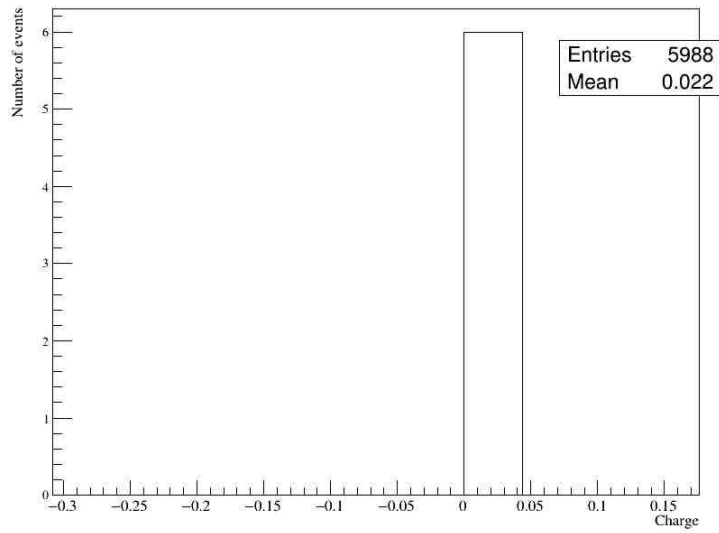


Fig 3-30 Number of events with charge (0) in beryllium from bremsstrahlung radiation.

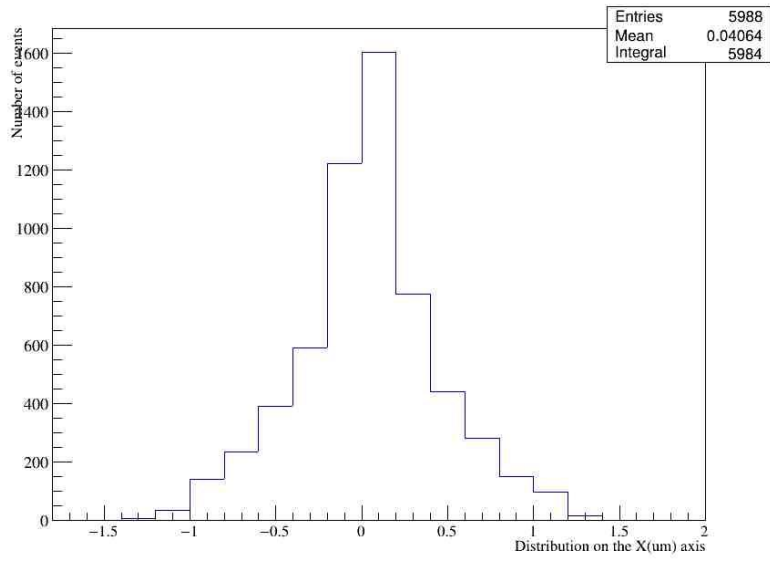


Fig 3-31 Distribution of electrons along the X axis in beryllium . Range of about 1.4mm.

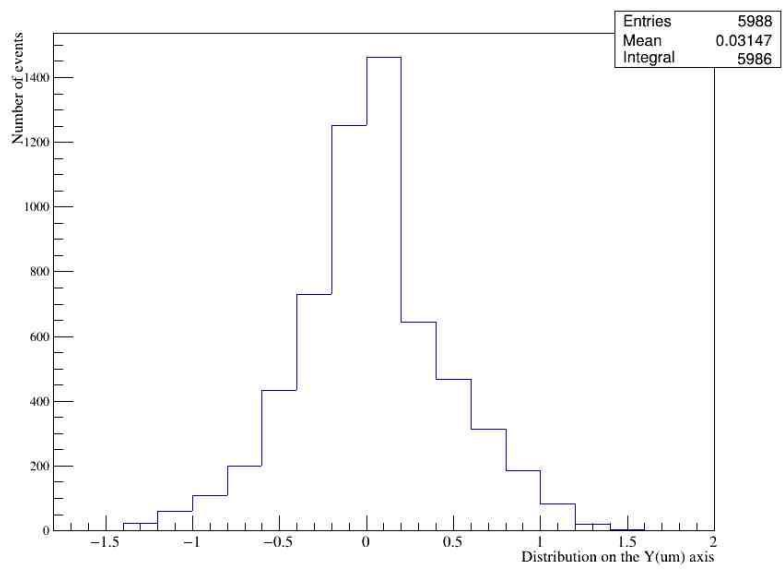


Fig 3-32 Distribution of electrons along the Y axis in beryllium . Range of about 1.4mm.

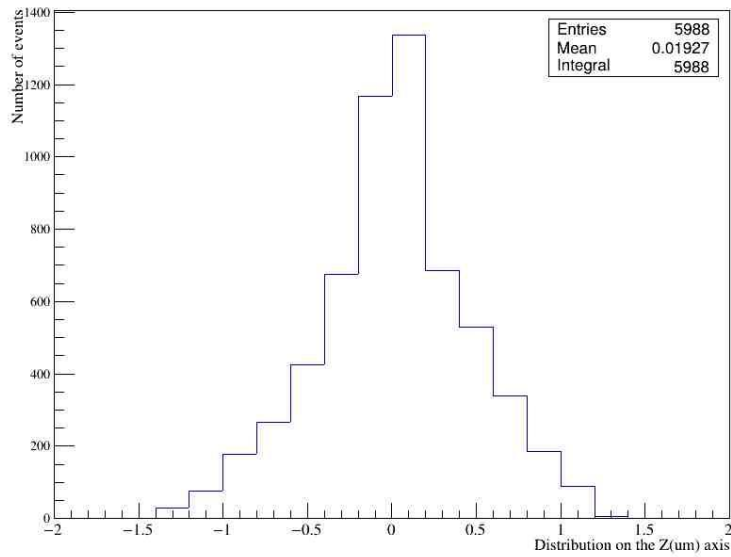


Fig 3-33 Distribution of electrons along the Z axis in beryllium . Range of about 1.2mm.

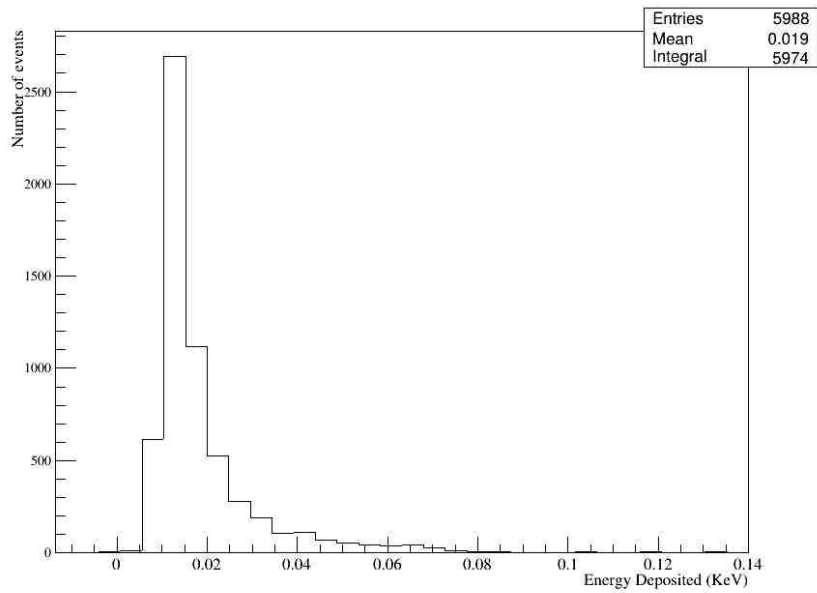


Fig 3-34 Energy Deposited by electrons in beryllium.

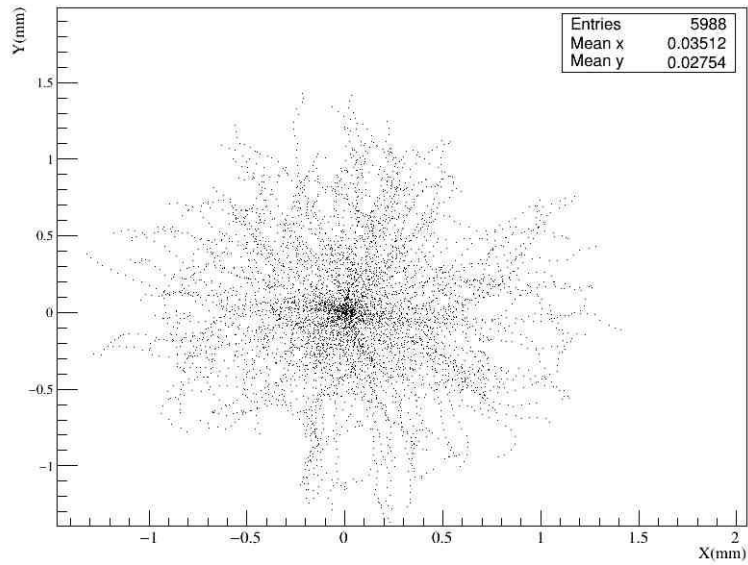


Fig 3-35 Tracks of electrons in beryllium projected on the XY plane.

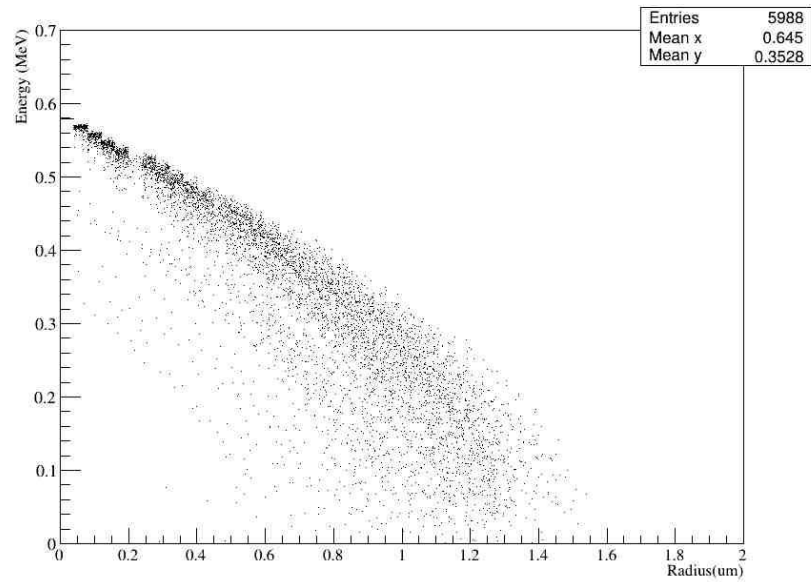


Fig 3-36 Kinetic energy of Electrons at various depth in beryllium.
B. Positrons

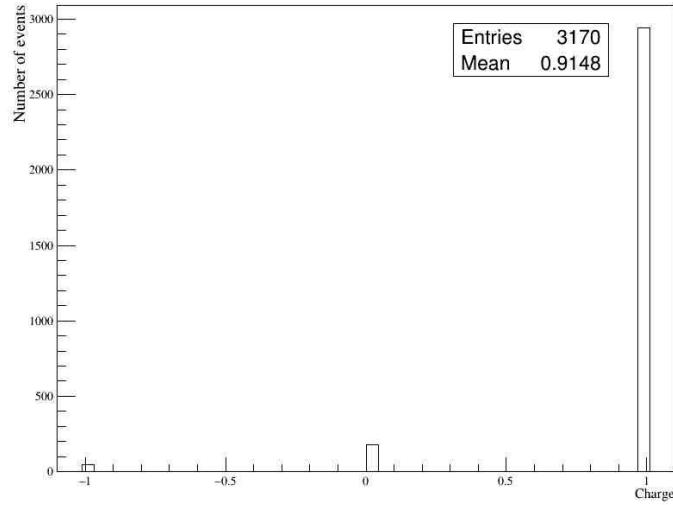


Fig 3-37 3170 events in total of which about 2900 were caused by primary positrons (charge 1) while about 220 events were caused by both secondary photons and electrons.

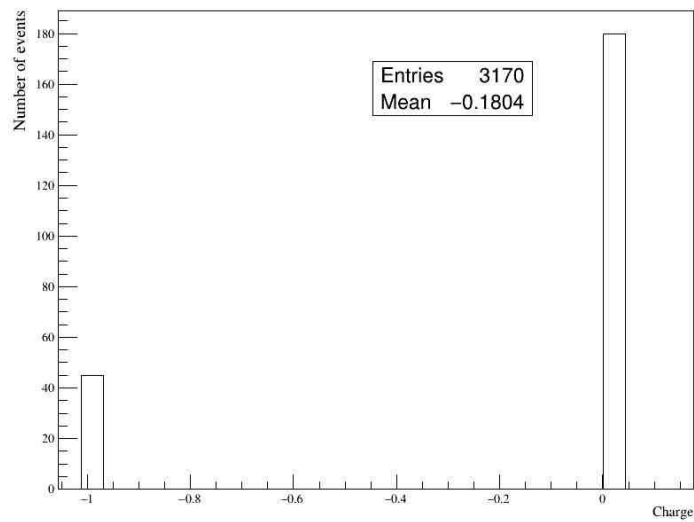


Fig 3-38 Fig. 3.36 zoomed in between -1 and 0, showing both gamma photons and secondary electron events.

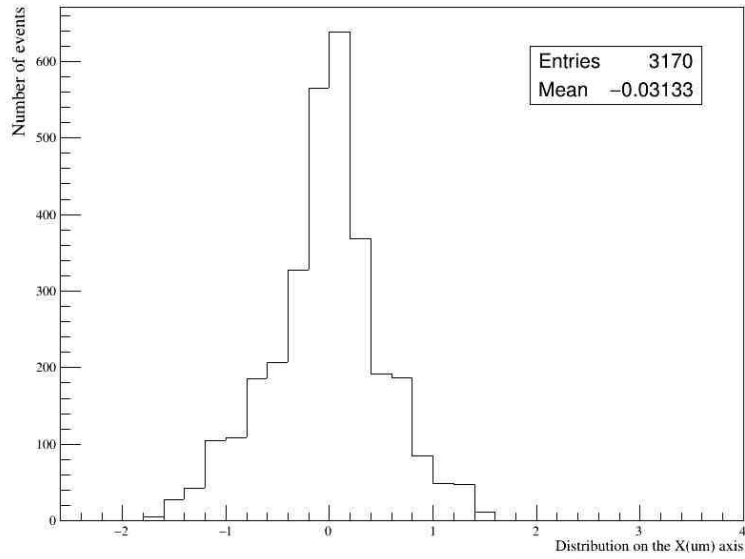


Fig 3-39 Distribution of Positrons along the X axis with a range of 1.6mm.

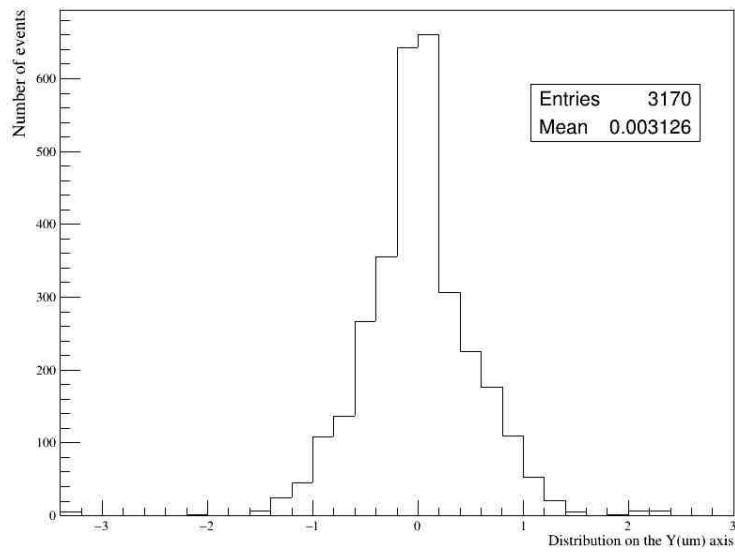


Fig 3-40 Distribution of Positrons along the Y axis with a range of 1.4mm.

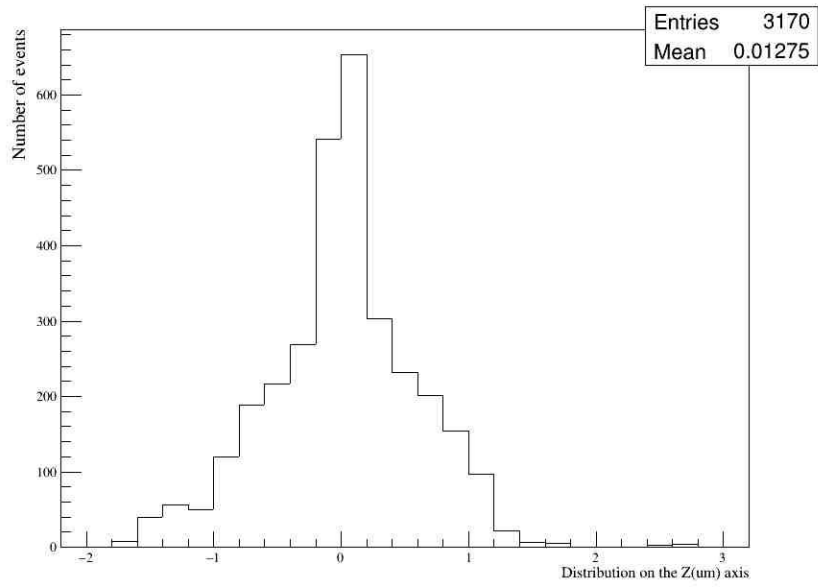


Fig 3-41 Distribution of Positrons along the Z axis with a range of 1.8mm.

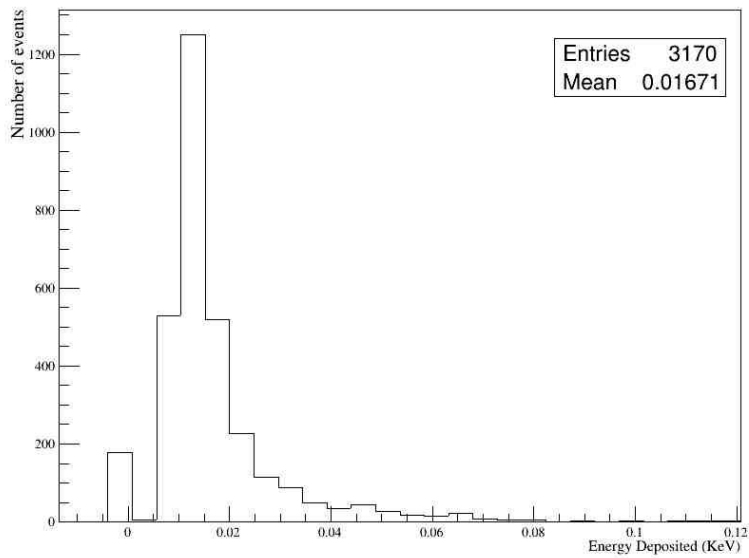


Fig 3-42 Energy deposited in beryllium for both electrons and positron events.

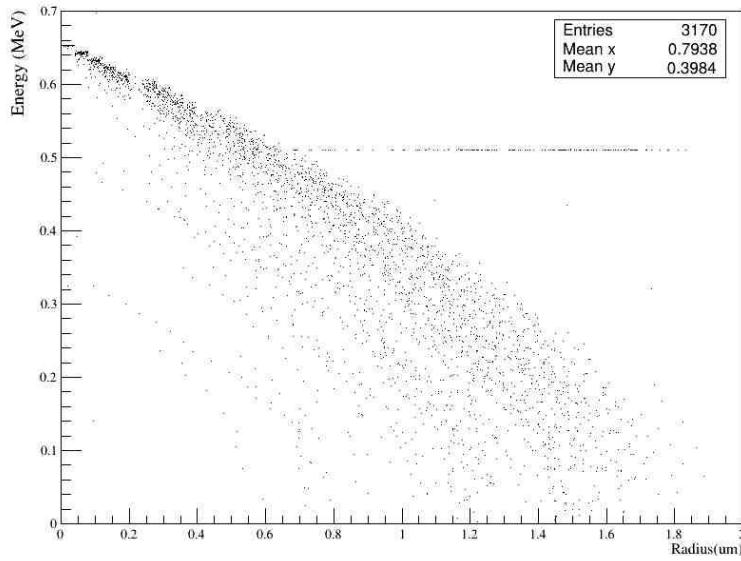


Fig 3-43 Kinetic energy of Positrons at various depth in in beryllium.

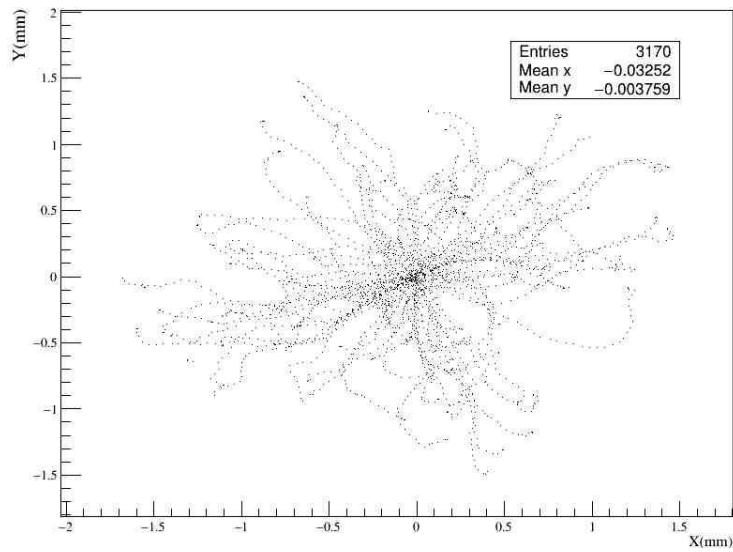


Fig 3-44 Tracks of 653 KeV positrons in beryllium projected on the XY plane.

3.2.4 Beta Particles in iron

For beta particles in iron, our results in Figures 3-45 to 3-58 shows the various events of beta particles in iron. Fig 3-45 shows the primary electron events in our simulation. In Fig 3-53, we see again a mixed field generated primarily from positron activities in iron. secondary γ photons and electrons events from annihilation and ionization events are suppressed due to the atomic mass of iron. This is also visible from Fig 3-47 to Fig 3-49, which shows the electrons quickly brought to rest after transversing about 0.2mm of iron. (the same can be said for positrons as shown in figures 3-54 to 3-56) thus the range of beta particles (between 579 KeV to 653 KeV) in iron is about 0.2mm.

Fig 3-51 and 3-58 is a plot of the kinetic energy of beta particles (electrons and positrons respectively) against the radial distance from the source. Beta particles from these figures transversed approximately 0.22 of iron before their KE was completely exhausted. This short distance is expected since iron has a large atomic number and is very dense. Fig. 3-50 as well as Fig 3-57 shows that a significant amount of energy is deposited by all the events in iron , unlike other materials we have seen so far. The tracks of electrons in iron as shown in figure 3-52 shows the path of the electrons as points. This again is due to the mass and density of iron as KeV beta particles are almost completely stopped as soon as they enter the material.

A. Electrons

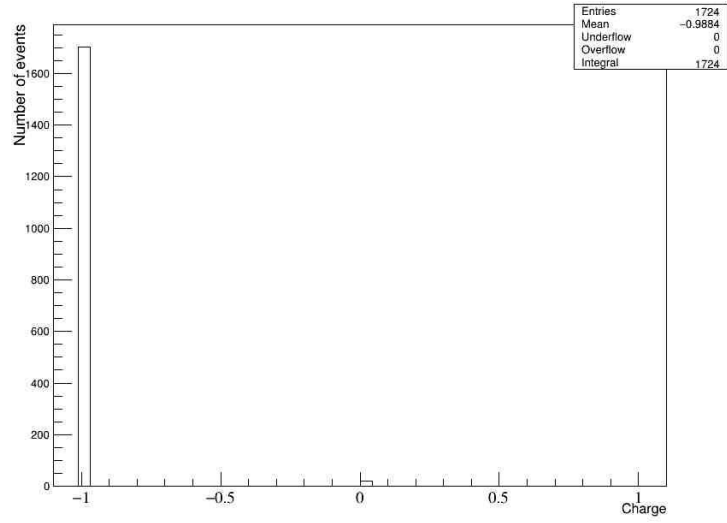


Fig 3-45 Number of events with charge (-1) in iron.

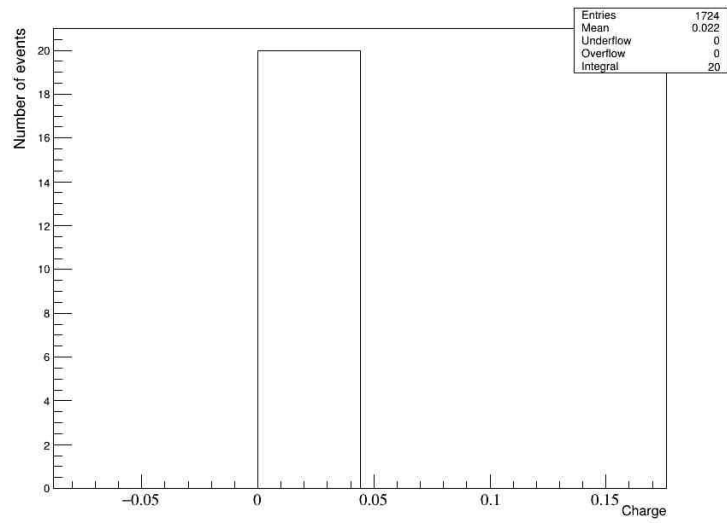


Fig 3-46 Number of events with charge (0) in iron from bremsstrahlung radiation.

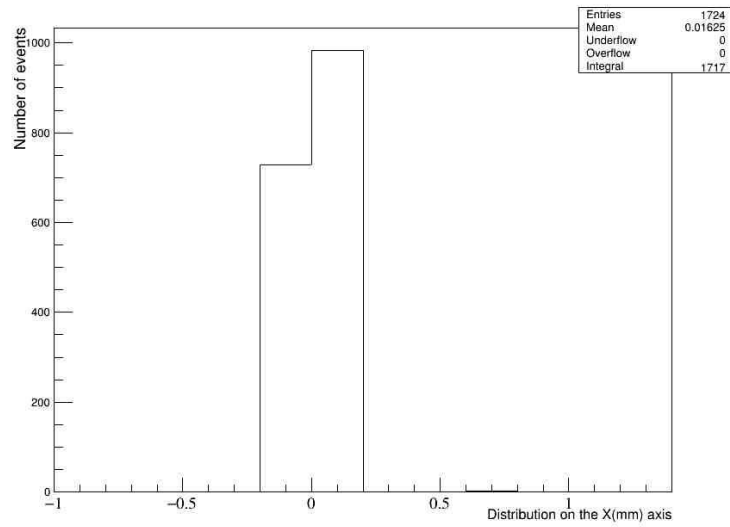


Fig 3-47 Distribution of electrons along the X axis in iron.

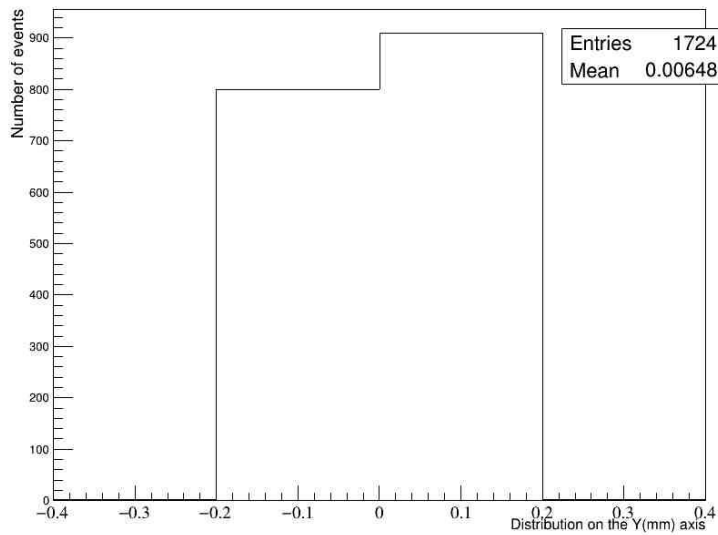


Fig 3-48 Distribution of electrons along the Y axis in iron.

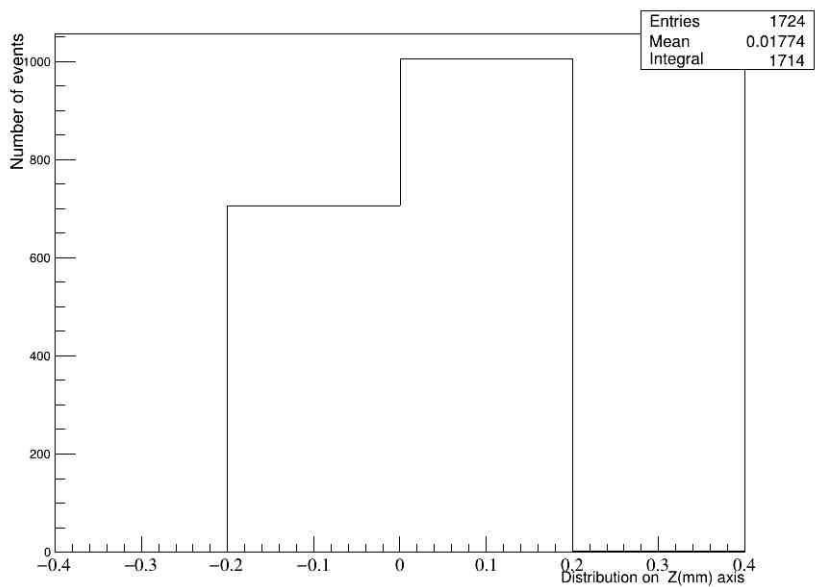


Fig 3-49 Distribution of electrons along the Z axis in iron.

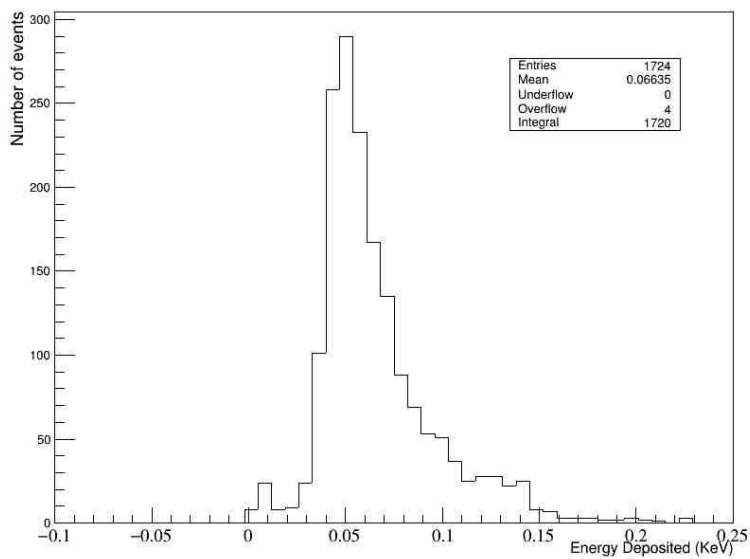


Fig 3-50 Energy Deposited by electrons in iron.

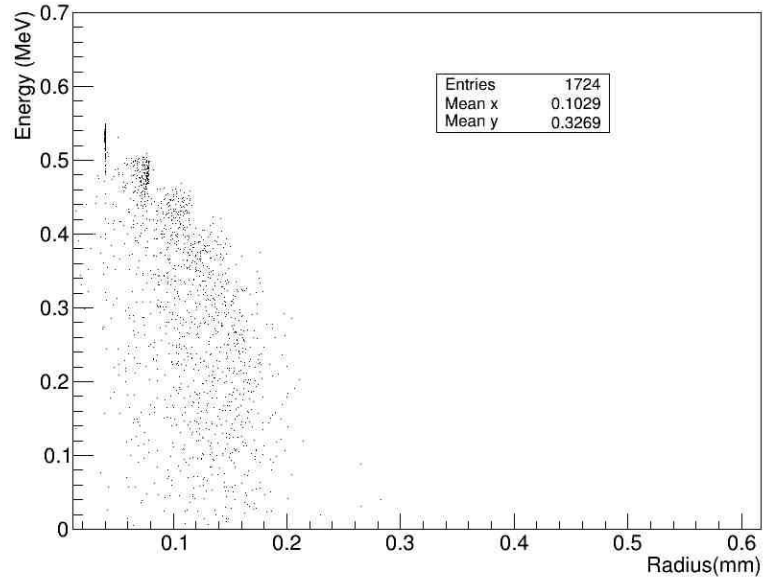


Fig 3-51 Kinetic energy of Electrons at various depth in iron.

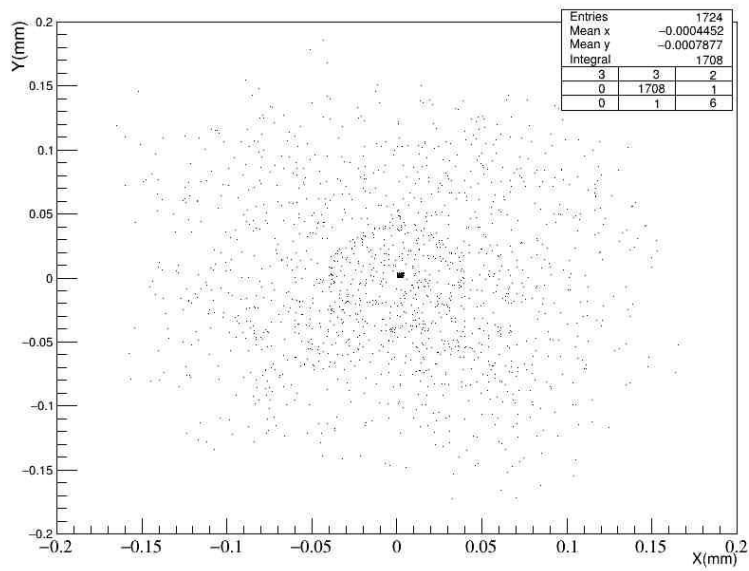


Fig 3-52 Tracks of electrons in iron projected on the XY plane.

B. Positrons

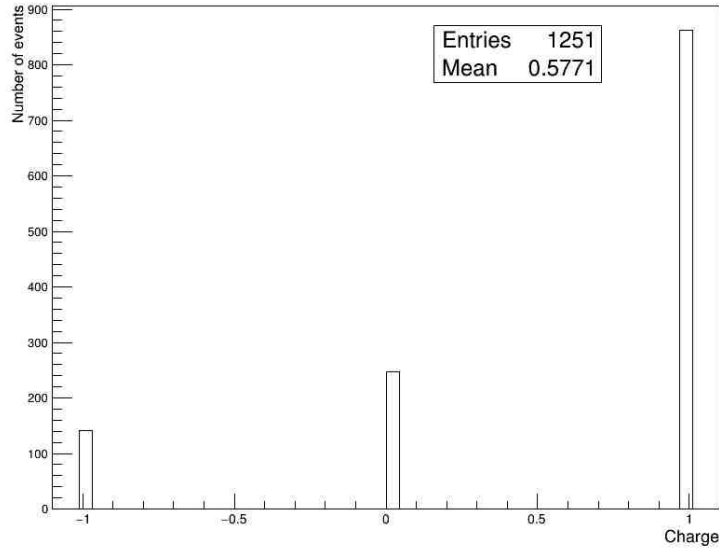


Fig 3-53 A mixed field of electrons, positrons and gamma photons generated from ionization, our simulation and annihilation processes respectively.

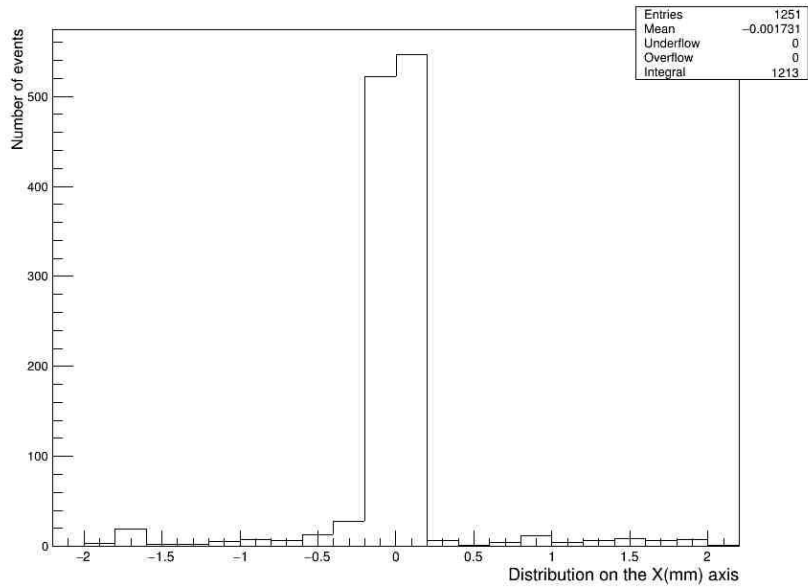


Fig 3-54 Distribution of Positrons along the X axis with a range of about 0.2 mm.

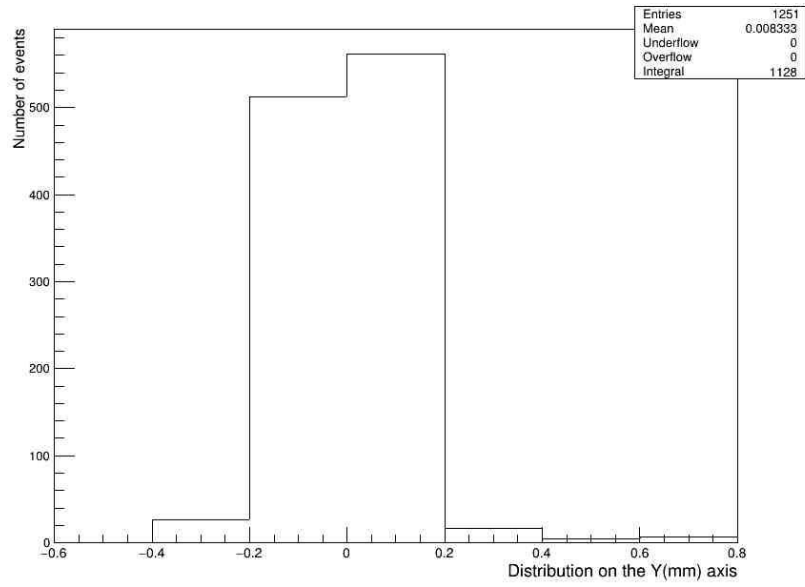


Fig 3.55 Distribution of Positrons along the Y axis with a range of about 0.2 mm.

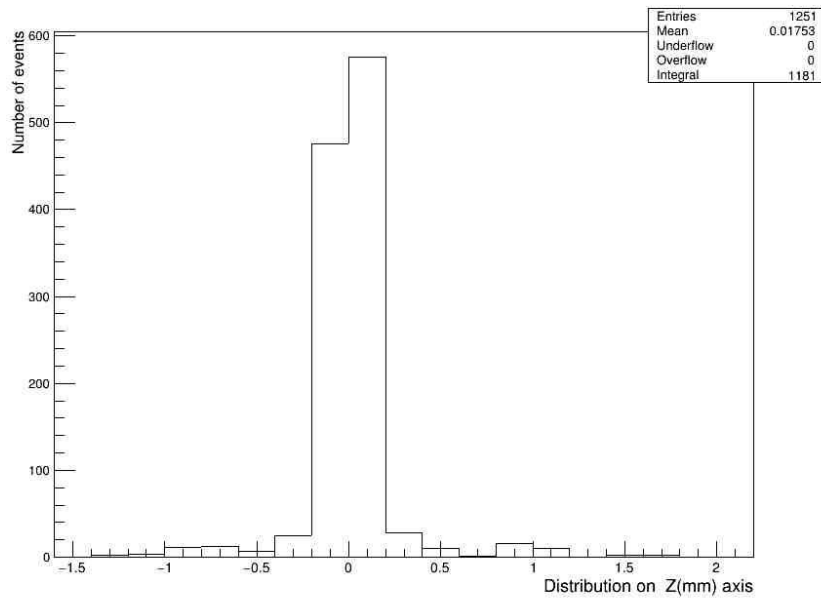


Fig 3-56 Distribution of Positrons along the Z axis with a range of about 0.2 mm.

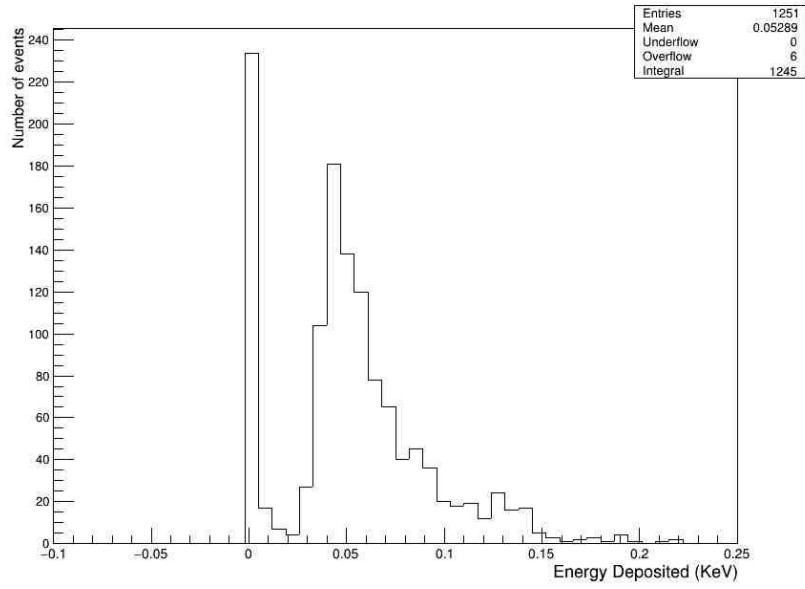


Fig 3-57 Number of events and corresponding Energy deposited in iron.

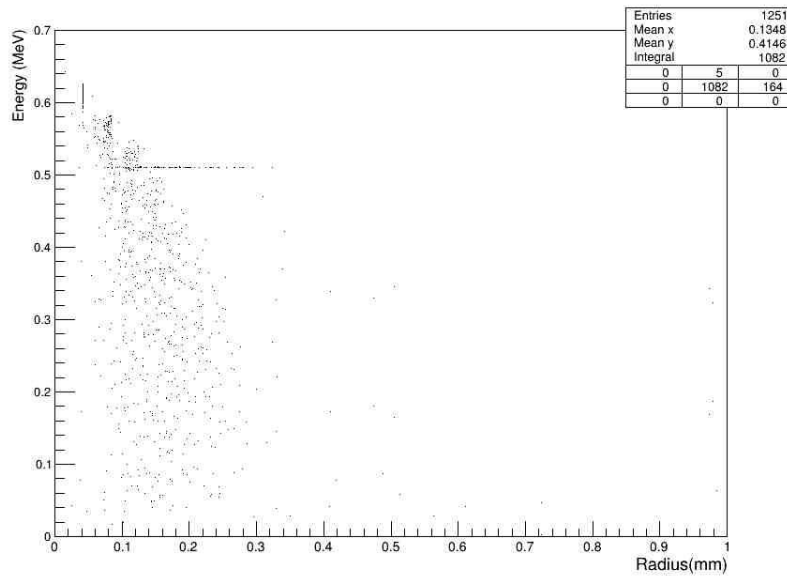


Fig 3-58 Kinetic energy of positrons in iron at various depth in iron.

3.2.5 Beta particles in Kapton

Lastly, here we have results from beta particles in kapton. From Fig 3-59, primary electron beams generated about 7 secondary γ photons (charge 0) as seen from Fig 3-60. For positrons in Fig 3-67 secondary γ photons and electrons were generated, again this constitute a mix field and could cause so much background noise in detecting beta particles outside the range. But compared to other materials, kapton seem very promising as a detector material for detecting beta particles because of the significant secondary events generated by each beta particle. Further more, Figures 3-61 to 3-63 as well as figures 3-69 to 3-71 shows the range of beta particles in iron. Electrons transverse about 1.4mm while positrons travel about 1.9mm. The energy deposited by both primary and secondary events in kapton can be seen from Fig 3-64 and Fig 3-72 for electrons and positrons respectively. This is further clarified Fig 3-65 and Fig 3-73 which is a plot of the kinetic energy of beta particles at different depths in kapton (about 1.9mm before energy reaches zero).

Finally the XY plane projection of the tracks of beta particles in kapton are shown in Fig 3-66 and Fig 3-74 for electrons and positrons respectively showing the 2D projection of beta particle tracks on the XY plane. Some tracks reveal almost a complete deflection of the incoming beta particles as a result of collision while others show continuous scattering at various angles in kapton.

Because the energy spectrum of the beta particles emitted by CU-64 (652.834 KeV) and F-18 (633.023 KeV) are almost the same, our simulations of positrons in various materials could represents the decay of F-18.

A. Electrons;

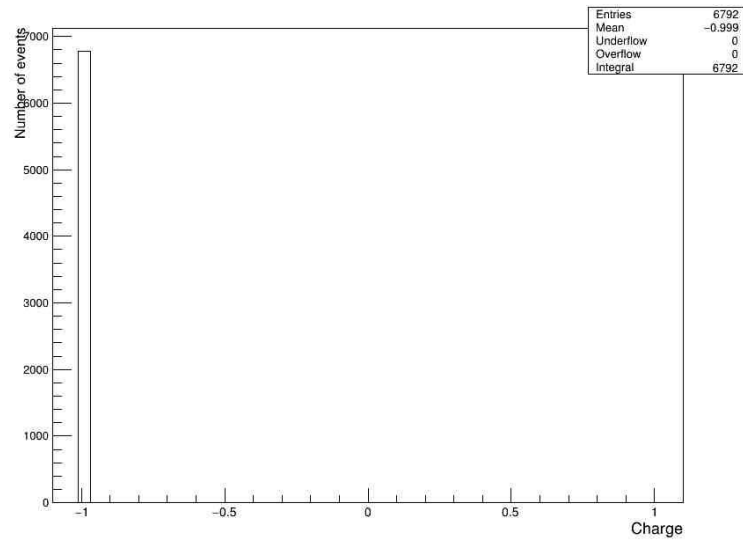


Fig 3-59 Number of events with charge (-1) in Kapton.

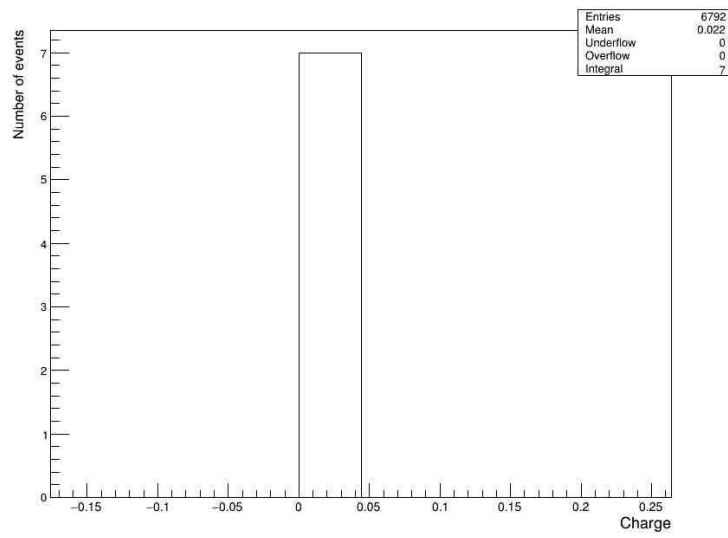


Fig 3-60 Number of events with charge (0) in kapton from bremsstrahlung radiation.

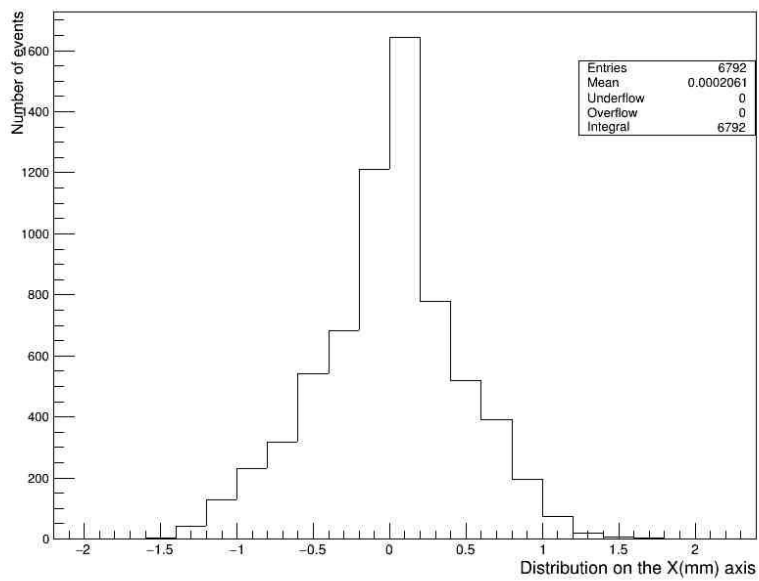


Fig 3-61 Distribution of electrons along the X axis in kapton.

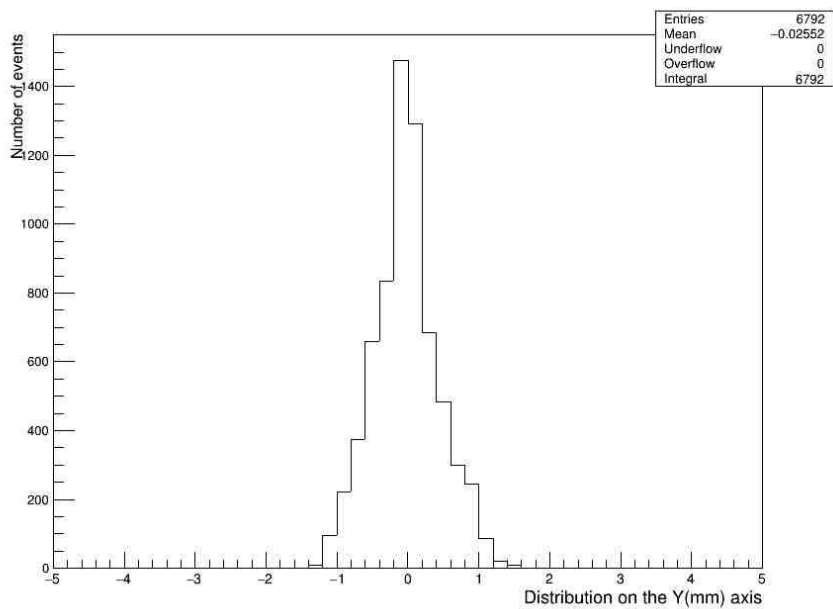


Fig 3-62 Distribution of electrons along the Y axis in kapton.

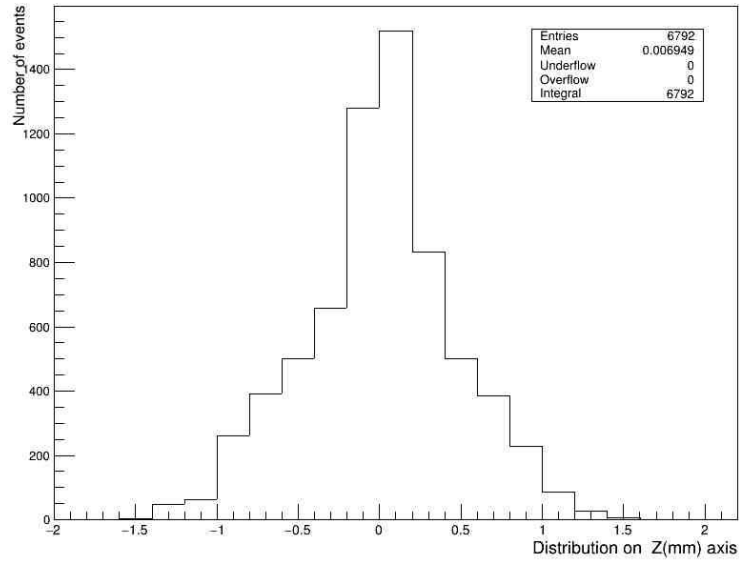


Fig 3-63 Distribution of electrons along the Z axis in kapton.

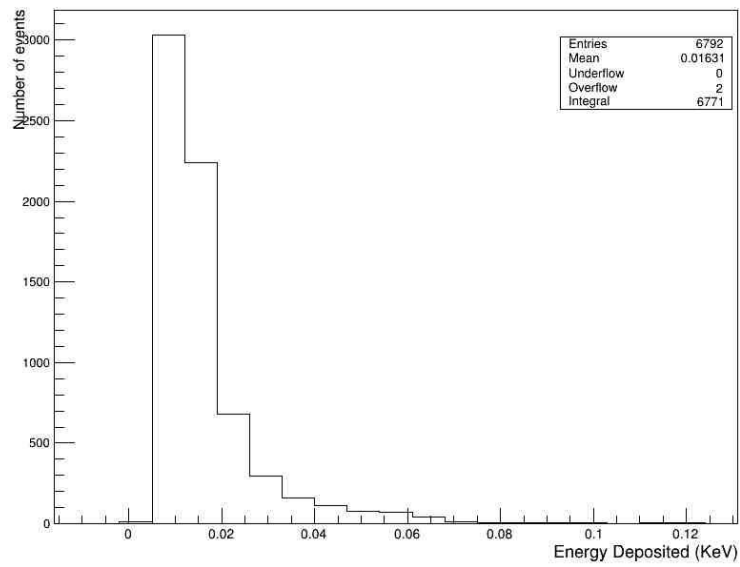


Fig 3-64 Energy Deposited by electrons in kapton.

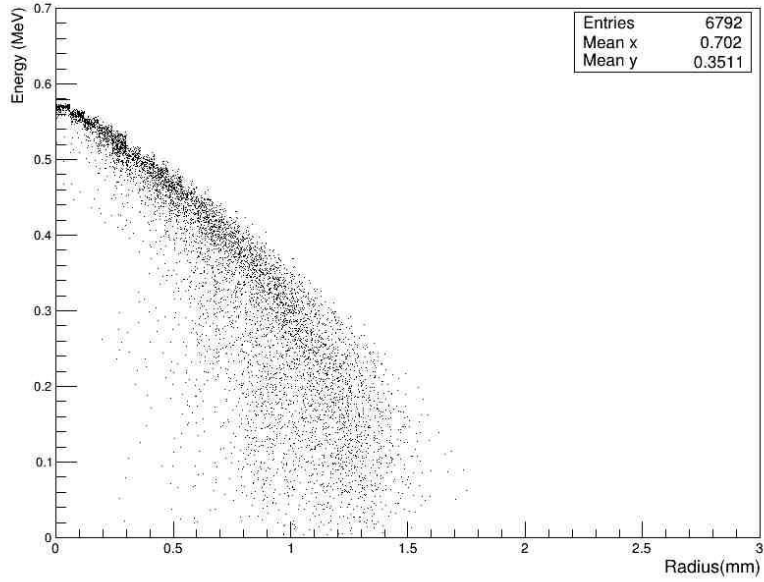


Fig 3-65 Kinetic energy of electrons at various depth in kapton.

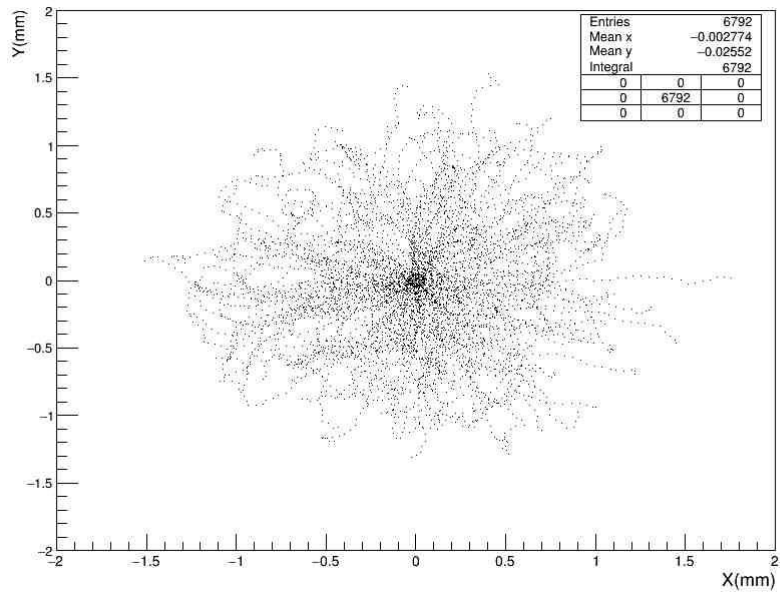


Fig 3-66 Tracks of electrons projected on the XY plane.

B. Positrons

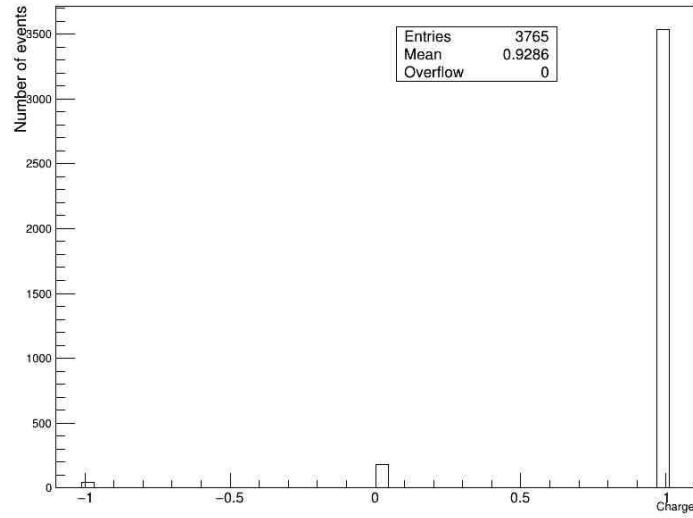


Fig 3-67 A mixed field of electrons, positrons and gamma photons.

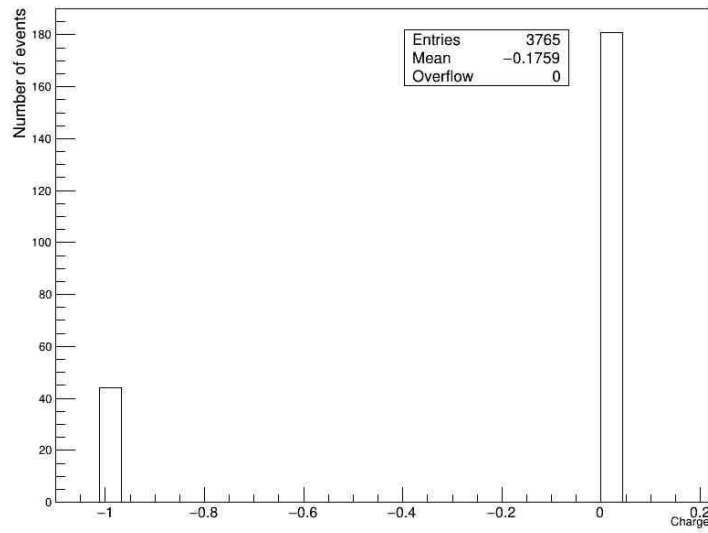


Fig 3.68 A blow up of Fig 3.66 between -1 and 0.

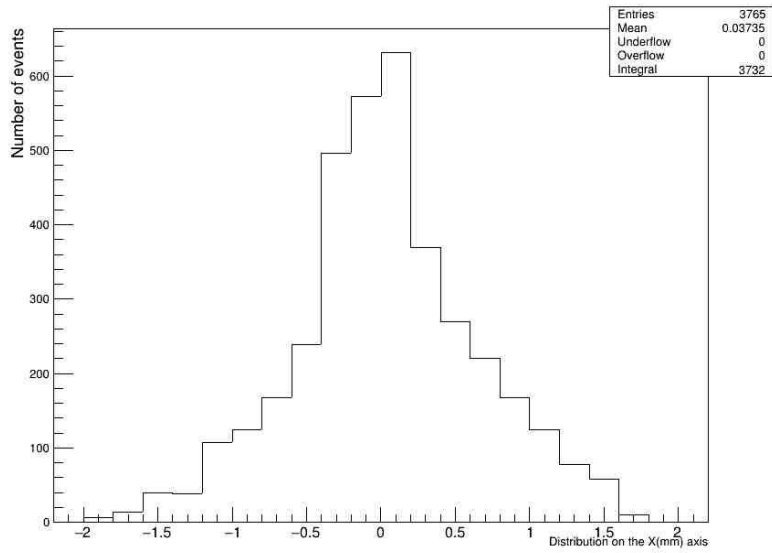


Fig 3-69 Distribution of Positrons along the X axis.

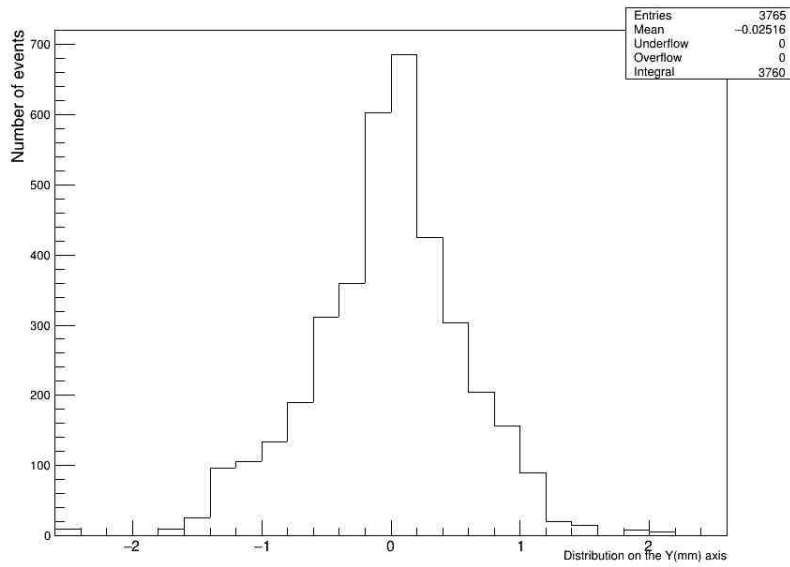


Fig 3-70 Distribution of Positrons along the Y axis.

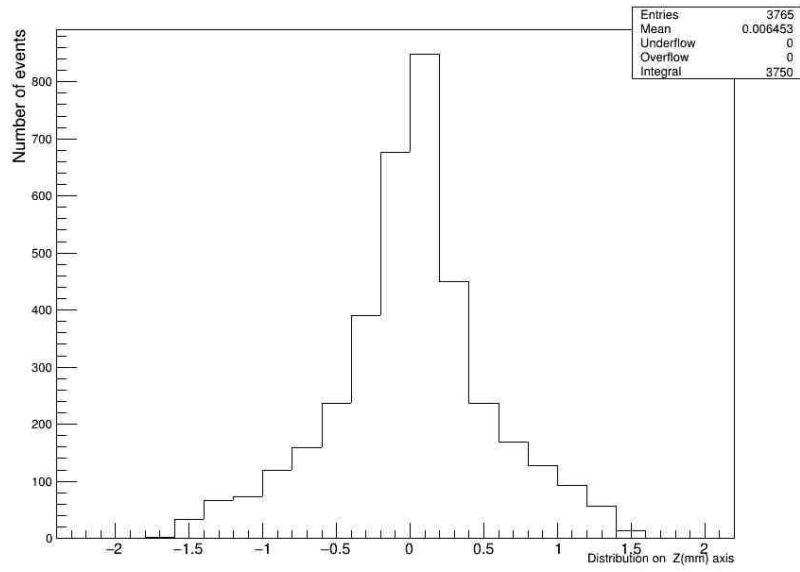


Fig 3-71 Distribution of Positrons along the Z axis.

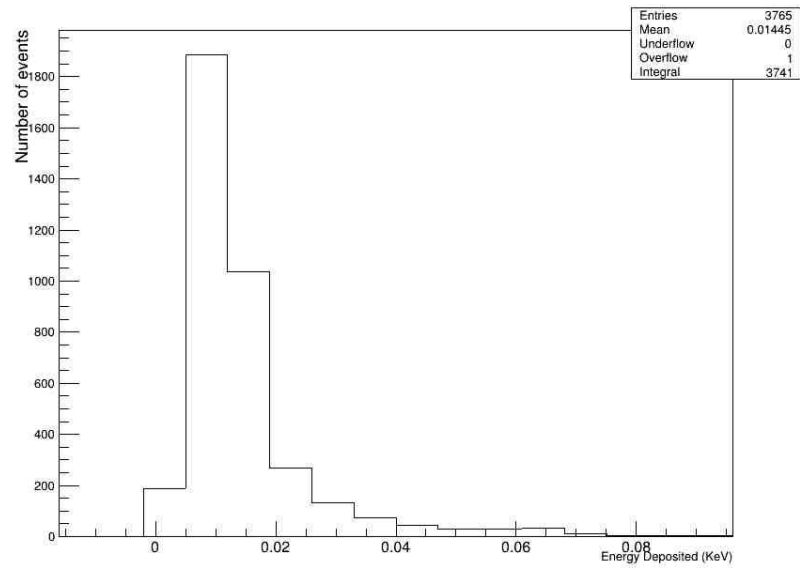


Fig 3-72 Energy Deposited by positrons in kapton.

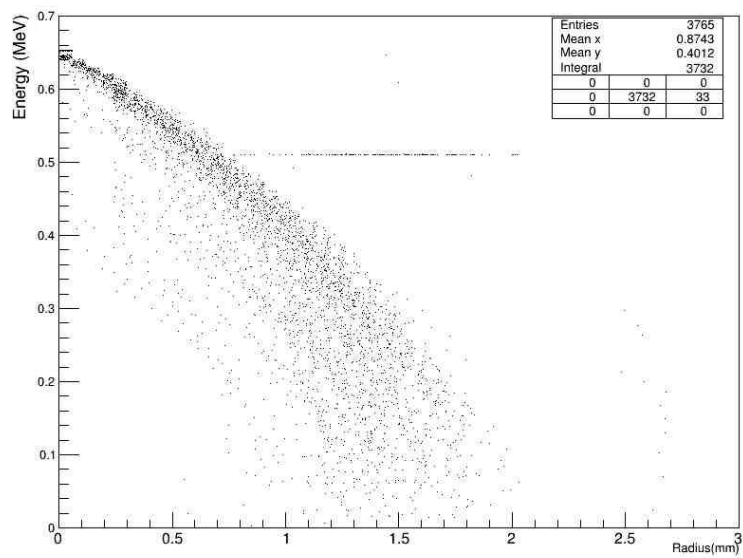


Fig 3-73 Kinetic energy of positrons at various depth in kapton.

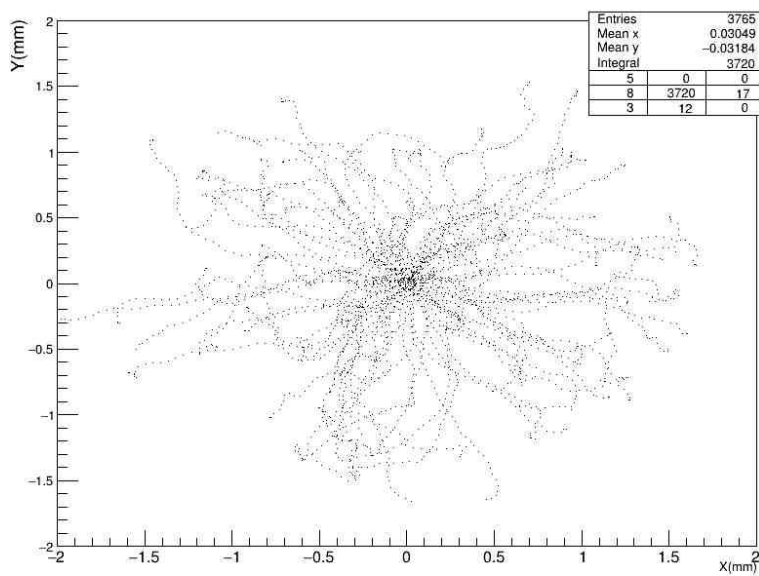


Fig 3-74 Tracks of 653 KeV positrons in kapton projected on the XY plane.

Chapter 4

Conclusion

Radioisotopes like ^{64}Cu and ^{18}F are used to label molecules of interest (tracers) which are injected in small amount into a patient for clinical examinations and medical research in vivo. The tracer will distribute in the body according to its particular physiological pathway and its distribution can be imaged in a PET or SPECT scanner by measuring and localizing the two gamma-rays (one for SPECT) originating from the annihilation of the positron emitted by the radioisotopes.

Most of the clinical PET/ SPECT studies today use F-FDG and Cu-ATCM as a radiotracer, as this allows measuring glucose metabolism, which is known to be significantly enhanced in most tumor cells. Although combining these imaging modalities with CT scanners have improved the anatomical details of the reconstructed images, these imaging devices still have a limitation on the size of tumor detectable. This is partly due to the distance between the gamma camera and the source of radiation coming from the radiopharmaceutical administered to the patient and the weak signals emitted by small tumors. Hence improving these imaging techniques would require both increasing the sensitivity of the detectors as well as increasing the radiation dose on the patient; this could substantially increase the damage to healthy tissue. To keep the radiation dose as low as possible and enhance the details of the resulting images there is a need for a shift from the tomographic imaging devices to portable close-range surface imaging devices that could detect the beta particles emitted from radiopharmaceuticals.

This thesis is focused on the study of these radioisotope (^{64}Cu) with simulations and the evaluation of the properties of the beta particles emitted during their

decay in soft tissue and some select materials using the GEANT4-MC simulation toolkit. Monte Carlo (MC) methods give us a chance to estimate tracks, range in materials and distribution of KeV beta particles without having to perform the actual experiment or build detectors. The results of the various energies and range of beta particles in matter are summarized in table 4.0:

Table 4.1 Summary of results obtained from simulation, showing the range of beta particles in various materials

Element/ substance	β^+ energy (MeV)	β^- energy (MeV)	β^+ range (mm)	β^- range (mm)
Air	0.653	0.579	N/A	N/A
Water	0.653	0.579	2.00	1.80
Beryllium	0.653	0.579	1.50	1.40
Kapton	0.653	0.579	1.99	1.70
Iron	0.653	0.579	0.18	0.17

In this thesis we created a 1cmx 1cm x 1cm simulation environment, placed a radiation source at the center (0,0,0) of our simulation environment and randomly generated beta particles of the same energy and percentage as would be produced by a typical Cu- 64 decaying.

The environment is then filled with several materials (one at a time). The tracks of the beta particles are collected in a separate ROOT file for further analysis. The ROOT file generated was structured to collect data for the radius from the center, X Y Z displacement, Theta , Phi , kinetic energy and energy deposited by each of the events in the simulated environment in steps of 0.05mm. Sensitivity of the simulation environment was optimized to collect information of the gamma photons emitted from annihilation

and bremsstrahlung processes between the beta particles and the material in question. These gammas represent the crux of this work as we aim for portable imaging devices that could detect beta particles at a certain range; we also would like to know how much of the signals received by the detector are actual beta particles and not gamma photons which in this case constitute the background.

This thesis shows that GEANT4-MC is a powerful tool for simulating particle transportation in matter and the data obtained from this thesis could be further refined and used for the algorithms in future surface imaging devices.

4.1 Future work

In view of possible future developments in nuclear imaging, and the foundation established in this work, one way forward would be to simulate a complete unit which would involve all the elements individually considered in this work as a unit (both source and detector). The future simulation environment would have a particle source embedded water (representing human tissue of skin thickness) and a GEM detector placed right on the surface to detect the emerging beta particles. The GEM detector in this case would use beryllium, stainless steel, kapton and copper as the composite materials. Sensitivity of the detector to beta particles could be adjusted and the background noise reduced. This next step would open new insight to the future detection of beta particles for nuclear medicine.

References

- [1] Ollinger, J.M., Fessler, J.A., 1997. Positron-emission tomography. *Signal Processing Magazine, IEEE* 14,
- [2] Zanzonico, P., 2004. Positron emission tomography: a review of basic principles, scanner design and performance, and current systems. *Seminars in Nuclear Medicine* 34.
- [3] Zanzonico, P., Heller, S., 2007. Physics, instrumentation, and radiation protection, in: Biersack, H.-J., Freeman, L.M. (Eds.), *Clinical Nuclear Medicine*. Springer Berlin Heidelberg, Berlin, Heidelberg, pp. 1
- [4] Hoffman E. J., M. P. Tornai, M. Janecek, B. E. Pratt, and J. S. Iwanczyk, "Intraoperative probes and imaging probes," *Eur. J. Nucl. Med.*, vol. 26, no. 8, pp. 913–935, 1999.
- [5] Wernick MN, Aarsvold JN, *Emission tomography – the fundamentals of PET and SPECT*, Elsevier Academic Press, New York, 2004.
- [6] [Ammirati M](#), [Vick N](#), [Liao YL](#), [Ciric I](#), [Mikhael M](#) Effect of the extent of surgical resection on survival and quality of life in patients with supratentorial glioblastomas and anaplastic astrocytomas. [Neurosurgery](#). 1987;21(2):201-6.
- [7] [Jang JY](#), [Kim SW](#), [Park DJ](#), [Ahn YJ](#), [Yoon YS](#), [Choi MG](#), [Suh KS](#), [Lee KU](#), [Park YH](#). Actual long-term outcome of extrahepatic bile duct cancer after surgical resection. [Ann Surg](#). 2005;241(1):77-84.
- [8] [McGirt MJ](#), [Chaichana KL](#), [Attenello FJ](#), [Weingart JD](#), [Than K](#), [Burger PC](#), [Olivi A](#), [Brem H](#), [Quinoñes-Hinojosa A](#). Extent of surgical resection is independently associated with survival in patients with hemispheric infiltrating low-grade gliomas. [Neurosurgery](#). 2008;63(4):700-7
- [9] MacDonald LR, Tornai MP, Levin CS, Park J. Atac M, Cline DB, Hoffman EJ. Investigation of the physical aspects of beta imaging probes using scintillating fibers and visible light photon counters. *IEEE Trans. Nucl. Sci.* 1995;42: 1351-57.
- [10] Tornai MP, Patt BE, Iwanczyk JS, Tull CR, MacDonald LR, Hoffman EJ. A novel silicon array designed for intraoperative charged particle imaging. *Med Phys*. 2002 Nov;29(11):2529-40.
- [11] Tipnis S. V., V. V. Nagarkar, I. Shestakova, V. Gaysinskiy, G. Entine, M. P. Tornai, and B. C. Stack, Jr. Feasibility of a Beta-Gamma Digital Imaging Probe for Radioguided Surgery. *IEEE Trans. Nucl. Sci.* 2004; 51:110-6
- [12] Strong VE, Galanis CJ, Riedl CC, Longo VA, Daghighian F, Humm JL, Larson SM,

- Fong Y. Portable PET probes are a novel tool for intraoperative localization of tumor deposits. *Ann Surg Innov Res.* 2009 Feb 21;3:2.
- [13] Meyerhof, WE. *Elements of nuclear physics.* McGraw-Hill, New York, 1967.
- [14] Li Y, Lu W, Huang Q, Huang M, Li C, Chen W. Copper sulfide nanoparticles for photothermal ablation of tumor cells. *Nanomedicine (Lond).* 2010 Oct;5(8):1161-71.
- [15] Zhou M, Zhang R, Huang M, Lu W, Song S, Melancon MP, Tian M, Liang D, Li C. A chelator-free multifunctional [64Cu]CuS nanoparticle platform for simultaneous micro-PET/CT imaging and photothermal ablation therapy. *J Am Chem Soc.* 2010 Nov 3;132(43):15351-8.
- [16] Kubota, K., 2001. From tumor biology to clinical Pet: a review of positron emission tomography (PET) in oncology. *Annual Nuclear Medicine* 15,
- [17] Couturier, O., Luxen, A., Chatal, J.-F., Vuillez, J.-P., Rigo, P., Hustinx, R., 2004. Fluorinated tracers for imaging cancer with positron emission tomography. *European Journal of Nuclear Medicine and Molecular Imaging* 31, 1182–1206.
- [18] Larson, S.M., Schwartz, L.H., 2006. 18 F-FDG PET as a candidate for “qualified biomarker”: functional assessment of treatment response in oncology. *Journal of Nuclear Medicine* 47.
- [19] Guhlke, S., Verbruggen, A.M., Vallabhajosula, S., 2007. Radiochemistry and Radiopharmacy, in: Biersack, H.-J., Freeman, L.M. (Eds.), *Clinical Nuclear Medicine.* Springer Berlin Heidelberg, Berlin, Heidelberg, pp. 34–76.
- [20] Buvat, I., Lazaro, D., 2006. Monte Carlo simulations in emission tomography and GATE: An overview. *Nucl. Instr. and Meth.* 569, 323– 329.
- [21] Salvat, F., Fernandez-varea, D., Sempau, J., 2008. PENELOPE-2008: A code system for Monte Carlo simulation of electron and photon transport.
- [22] Agostinelli, S., Allison, J., Amako, K., Apostolakis, J., Araujo, H., et al., 2003. Geant4—a simulation toolkit. *Nuclear Instruments and Methods in Physics Research Section A: Accelerators, Spectrometers, Detectors and associated equipment* 506, 250
- [23] Briesmeister, J.F., 1993. MCNP 4 A, Monte Carlo code for N-particle transport system. New Mexico, Los Alamos National Laboratory.
- [24] Kawrakow, I., Bielajew, A.F., 1998. On the condensed history technique for electron transport. *Nucl. Instr. Meth. B:* 142, 253–280.
- [25] Harrison, R.L., Dhavala, S., Kumar, P.N., Shao, Y., Manjersshwar, R., Lewellen, T.K., Jansen, F.P., 2002. Acceleration of SimSET photon history generation, in: *Nuclear*

Science Symposium Conference Record, 2002 IEEE. pp. 1835–1838.

[26] Thompson, C.J., Moreno-Cantu, J., Picard, Y., 1992. PETSIM: Monte Carlo simulation of all sensitivity and resolution parameters of cylindrical positron imaging systems. *Physics in medicine and biology* 37, 731.

[27] Zaidi, H., 1999. Relevance of accurate Monte Carlo modeling in nuclear medical imaging. *Medical Physics* 26,574.

[28] Jan, S., Santin, G., Strul, D., Staelens, S., Assie, K., Autret, D., Avner, S., Barbier, R., Bardies, M., Bloomfield, P.M., others, 2004. GATE: a simulation toolkit for PET and SPECT. *Physics in medicine and biology* 49, 4543.

[29] Glen F. Knoll, *Radiation Detection and Measurement*, edition 5, 1989

[30] Assié, K., Breton, V., Buvat, I., Comtat, C., Jan, S., Krieguer, M., Lazaro, D., Morel, C., Rey, M., Santin, G., Simon, L., Staelens, S., Strul, D., Vieira, J.-M., Walle, R.V.de, 2004. Monte Carlo simulation in PET and SPECT instrumentation using GATE. *Nuclear Instruments and Methods in Physics Research Section A*:

[31] Cherry, S.R., Sorenson, J.A., Phelps, M.E., 2003. *Physics in Nuclear Medicine*, 3rd revised edition. ed. Saunders (W.B.) Co Ltd

[32] Krane, K.S., 1987. *Introductory Nuclear Physics*, 3rd ed. Wiley, New York.

[33] E.B Podgorsak *Radiation Physics for medical physicist*, Springer , Newyork, 2006

[34] Khadijeh P. Optimization of plastic scintillator thickness for Beta online Beta detection in mixed fields. Ontario 2010 Dec. :29-34

[35] Geoffrey G.Eichholz , John W.Poston. *Principles of Nuclear Radiation Detection* ,1985

[36] F. Sauli. Gem: A new concept for electron amplification in gas detectors. *Nucl. Instr. Meth. A* , 386 1997.

[37] Nicholas Tsoufanidis, *Measurement and Detection of Radiation*, 1995

[38] Agostinelli, S., Allison, J., Amako, K., Apostolakis, J., Araujo, H., et al., 2003. Geant4—a simulation toolkit. *Nuclear Instruments and Methods in Physics Research Section A: Accelerators, Spectrometers, Detectors and associated equipment* 506, 250–303

[39] Baro, J., Sempau, J., Fernández-Varea, J.M., Salvat, F., 1995. *Nucl. Instr. Meth. in Physics Research Section B: Beam Interactions with Materials and Atoms* 100, 31–46

[40] Andreo, P., 1991. Monte Carlo techniques in medical radiation physics. *Physics in Medicine and Biology* 36

[41] W.R.Leo. *Techniques for Nuclear and Particle Physics Experiments, Second Revised Edition*, second edition, 1993

[42] España, S., 2009. Simulaciones avanzadas aplicadas al diseño de escáneres y mejora de la calidad de imagen en tomografía por emisión de positrones. Doctoral dissertation, Madrid, Universidad Complutense de Madrid.

Biography

Bright Izudike earned his bachelors degree from the university of Jos in Nigeria in 2012, and in 2015 he was awarded a master of science degree from the university of Texas at arlington USA.

Since 2010 Bright engaged in several researches which include determining the radiation levels around the Jos University Teaching Hospital in jos, investigating the humidity of Jos University area from the saturation vapor pressure. He also has theoretically determined the mass of the Higgs bosson (for the LHC running at 13.0 TeV) with the High energy group at UTA. Currently working in collaboration with the high energy physics group in UTA, his research in nuclear imaging will pave way for future portable imaging devices that could replace the conventional imaging techniques available in clinics. He hopes to pursue his PhD in medical physics in the future.